Inorganica Chimica Acta 522 (2021) 120358

Contents lists available at ScienceDirect

Inorganica Chimica Acta

journal homepage: www.elsevier.com/locate/ica

Research paper

A novel family of hepta-coordinated Cr(III) complexes with a planar pentadentate N_3O_2 Schiff base ligand: synthesis, structure and magnetism

T.A. Bazhenova [a], L.V. Zorina [b,*], S.V. Simonov [b], Yu.V. Manakin [a], A.B. Kornev [a], K.A. Lyssenko [c], V.S. Mironov [a,d,*], I.F. Gilmutdinov [e], E.B. Yagubskii [a,*]

[a] Institute of Problems of Chemical Physics, IPCP RAS, Chernogolovka, Russia
[b] Institute of Solid State Physics, ISSP RAS, Chernogolovka, Russia
[c] Department of Chemistry, Lomonosov Moscow State University, Moscow, Russia
[d] Shubnikov Institute of Crystallography of Federal Scientific Research Centre "Crystallography and Photonics" RAS, Moscow, Russia
[e] Institute of Physics, Kazan Federal University, Kazan, Russia

ARTICLE INFO

Keywords:
Pentagonal-bipyramidal Cr(III) complexes
Pentadentate Schiff-base ligands
Synthesis
Jahn-Teller effect
Magnetic properties
Zero-field splitting

ABSTRACT

A series of seven-coordinate pentagonal-bipyramidal (PBP) Cr(III) complexes with pentadentate pyridine-based ligands, 2,6-diacetylpyridine bis(4-methoxybenzoylhydrazone), $H_2DAPMBH$ (H_2L^{OCH3}) or 2,6-diacetylpyridine bis(benzoylhydrazone), H_2DAPBH (H_2L) and different axial ligands have been prepared. The reaction of the H_2L^{OCH3} with $CrCl_2{\cdot}4H_2O$ in methanol or $CrCl_3{\cdot}6H_2O$ in CH_3CN led to a novel seven-coordinate pentagonal-bipyramidal (PBP) complex $[Cr(HL^{OCH3})Cl_2]$ (**1**) with the mono-deprotonated chelating ligand in the equatorial plane and two apical Cl atoms. Then, taking advantage of lability of the apical Cl ligands in **1**, a number of PBP Cr^{III} complexes with charged (viz. CH_3O^-, N_3^-, CN^-, NCS^-) and neutral (viz. CH_3OH, H_2O) apical ligands was obtained and characterized: $[Cr(HL^{OCH3})Cl_2]{\cdot}4CHCl_3$ (**1**), $[Cr(HL^{OCH3})Cl_2]{\cdot}CH_3OH$ (**1a**), $[Cr(HL^{OCH3})(H_2O)Cl]PF_6{\cdot}CH_3OH$ (**2**), $[Cr(HL)(H_2O)Cl]ClO_4{\cdot}0.25H_2O$ (**3**), $[Cr(HL^{OCH3})(H_2O)_2](NO_3)_2{\cdot}H_2O{\cdot}C_2H_5OH$ (**4**), $[Cr(L^{OCH3})(CH_3OH)(OCH_3)]{\cdot}CH_3OH$ (**5**), $[Cr(HL^{OCH3})(NCS)_2]{\cdot}1.5H_2O$ (**6**), $[Cr(HL^{OCH3})(N_3)_2]{\cdot}xH_2O$ (**7**, x = 0.2, **8**, x = 0, **9**, x = 0, three phases in the same synthesis), $[Cr(L^{OCH3})(N_3)_2][Na(CH_3OH)_2]{\cdot}2CH_3OH$ (**10**), $[Cr(L^{OCH3})(CN)_2][Na(H_2O)(C_2H_5OH)]$ (**11**). Single crystal X-ray analysis reveals that all the complexes **1**–**11** have the PBP geometry with a pentadentate ligand in a form of $[HL^{OCH3}]^-$ or $[L^{OCH3}]^{2-}$ in the equatorial plane. The PBP complexes are prone to aggregate into dimers or polymers, either due to strong hydrogen bonds or due to the transformation of terminal ligands into bridging between different metallic centers. All complexes **1**–**11** exhibit considerable in-plane distortion of the CrN_3O_2 pentagon due to the shift of the Cr^{III} ion from the central position, which is caused by the strong first-order Jahn-Teller (JT) effect for the high-spin $3d^3$ configuration in the PBP ligand field. The mechanism of JT distortions is rationalized in terms of DFT calculations. DC magnetic measurements indicate a high-spin ($S = 3/2$) ground state of complex $[Cr(HL^{OCH3})Cl_2]{\cdot}4CHCl_3$ (**1**); theoretical analysis of its magnetic properties reveals negative zero-field splitting energy with the anisotropy parameter $D = -1.8$ cm^{-1} and weak dimer-like antiferromagnetic spin coupling $J = -0.23$ cm^{-1} between neighboring PBP units $[Cr^{III}(HL^{OCH3})Cl_2]$ mediated by π-stacking of planar H_2L^{OCH3} ligands.

1. Introduction

Coordination chemistry of chromium(III) compounds continues to attract great interest, both as an active field of fundamental research and due to development of new advanced functional materials for modern applications, such as efficient catalysts based on chromium complexes [1], photoactive materials [2,3] and molecule-based magnetic materials [4]. Currently, a huge number of various inorganic and organometallic chromium(III) coordination compounds, both mono- and polynuclear, have been isolated and characterized; in most of them, Cr^{III} ions are octahedrally coordinated. However, in recent years, the research interest has shifted towards transition-metal complexes with less-common coordination, trigonal–pyramidal [5–7], trigonal-prismatic [8–11] and pentagonal-bipyramidal [12–17]. Of these, pentagonal-bipyramidal (PBP) complexes are of special interest as spin carriers with strong Ising-type magnetic anisotropy [16–19]. These complexes are promising

* Corresponding authors.
E-mail addresses: zorina@issp.ac.ru (L.V. Zorina), mirsa@list.ru (V.S. Mironov), yagubski@icp.ac.ru (E.B. Yagubskii).

https://doi.org/10.1016/j.ica.2021.120358
Received 7 December 2020; Received in revised form 12 March 2021; Accepted 18 March 2021
Available online 23 March 2021

building units for the molecular design of new magnetic materials based on magnetically bistable low-dimensional coordination compounds featuring slow magnetic relaxation at low temperature, namely, single-molecule magnets (SMMs) and single-chain magnets (SCMs) [4,6–20]. In this respect, transition metal complexes with planar pentadentate macrocyclic ligands of the Schiff base type are especially attractive since they provide robust, nearly planar pentagonal coordination in the equatorial plane, which is supplemented by two apical ligands to form the PBP coordination polyhedron. Such complexes with high-spin 3d metal ions often exhibit substantial single-ion magnetic anisotropy with the zero-field splitting (ZFS) parameter *D* in the range of several tens of wavenumbers, as is the case for Fe(II) [16–18,20], Co(II) [15,16,18–20] and Ni(II) [16,20–22] complexes.

To date, numerous seven-coordinate PBP complexes with pentadentate Schiff base ligands have been obtained for almost all 3d transition metals [4,6–22]. By contrast, the number of chromium(III) PBP complexes is still very limited. Overall, the chemistry of Cr(III) complexes with such ligands is scarcely developed: in fact, there are only a few reports in the literature on crystallographically characterized PBP Cr(III) complexes with pentadentate Schiff base ligands. The first seven-coordinate Cr(III) complex was obtained in 1975 by Palenick et al. [23], when inorganic chemists still debated if such Cr(III) complexes could even exist. The authors of [23], and later in ref. [24] demonstrated the formation of PBP Cr(III) complex in the reaction of chromium nitrate with a pentadentate ligand with N_3O_2 chelating node, 2,6-diacetylpyridine-disemicarbazone, DAPSC. Recently, Sutter et al. [25–27] reported the synthesis of some new seven-coordinate PBP Cr(III) complexes with a similar pentadentate N_3O_2 ligand and successfully used them as metallo-ligand units for tailoring heterometallic molecule-based magnets. Besides, these PBP Cr(III) complexes exhibit considerable in-plane distortion of the CrN_3O_2 pentagon caused by the strong first-order Jahn-Teller effect for the high-spin $3d^3$ configuration [25–27].

One more important avenue of research of Cr(III) Schiff base complexes concerns their catalytic activity. In particular, chromium complexes with tetradentate N_2O_2 Schiff bases (such as salen) are known as efficient catalysts of the ring-opening copolymerization of epoxides and carbon dioxide, which are important for synthesis of aliphatic polycarbonates [28–32]. The search for new, more active and selective catalysts for this reaction is therefore an urgent task. In this regard, chemically related Cr(III) complexes with pentadentate Schiff bases may be promising as catalysts for the reaction of CO_2 with epoxides. Recently, we have started work in this direction and obtained some encouraging results; this work is currently underway [33].

Herein, we report synthesis and study of a series of new Cr(III) complexes with a pentadentate ligands, 2,6-diacetylpyridine bis(4-methoxybenzoylhydrazone), (H_2L^{OCH3}) or 2,6-diacetylpyridine bis (benzoylhydrazone), (H_2L) and with various apical ligands, $[Cr(HL^{OCH3})Cl_2]\cdot 4CHCl_3$ (**1**), $[Cr(HL^{OCH3})Cl_2]\cdot CH_3OH$ (**1a**), $[Cr(HL^{OCH3})(H_2O)Cl]PF_6\cdot CH_3OH$ (**2**), $[Cr(HL)(H_2O)Cl]ClO_4\cdot 0.25H_2O$ (**3**), $[Cr(HL^{OCH3})(H_2O)_2](NO_3)_2\cdot H_2O\cdot C_2H_5OH$ (**4**), $[Cr(L^{OCH3})(CH_3OH)(OCH_3)]\cdot CH_3OH$ (**5**), $[Cr(HL^{OCH3})(NCS)_2]\cdot 1.5H_2O$ (**6**), $[Cr(HL^{OCH3})(N_3)_2]\cdot xH_2O$ (**7**, x = 0.2, **8**, x = 0, **9**, x = 0, three phases in the same batch), $[Cr(L^{OCH3})(N_3)_2][Na(CH_3OH)_2]\cdot 2CH_3OH$ (**10**), $[Cr(L^{OCH3})(CN)_2][Na(H_2O)(C_2H_5OH)]$ (**11**). This study represents a part of our research activities aimed at designing new advanced molecular magnetic materials, which are based on new principles of the control of magnetic anisotropy [34–37]; the PBP 3d, 4d, 4f complexes with pentadentate Schiff base ligands are a key element of our strategy [38–43]. This paper describes investigations of the peculiarities of syntheses, crystallographic characterization and ligand-exchange reactions of a series of new Cr(III) complexes **1**–**11** with pentadentate ligand H_2L^{OCH3}. Magnetic measurements were done for compound **1** as a representative of the family of Cr(III) complexes **1**–**11**; its magnetic behavior is supplemented with a detailed theoretical analysis.

2. Experimental section

All manipulations involving air-sensitive materials ($CrCl_2\cdot 4H_2O$) were carried out under an argon atmosphere using the standard Schlenk-line method. Syntheses using Cr^{III} compounds as starting materials were performed under aerobic conditions. 2,6-diacetylpyridine, benzoylhydrazide, Et_3N, $CrCl_2\cdot 4H_2O$, $CrCl_3\cdot 6H_2O$, $Cr(NO_3)_3\cdot 9H_2O$, NaCN, NaN_3, 4-methoxybenzoic acid, thionyl chloride, hydrazine hydrate solution (50–60% N_2H_4), $NaOCH_3$ (solution in CH_3OH, Aldrich), $LiClO_4$, NH_4PF_6, NH_4CNS, were purchased from commercial sources and used without further purification. Methanol was dried upon refluxing with magnesium methoxide followed by distillation. Acetonitrile and chloroform were refluxed over calcium hydride and then distilled off. All the solvents were purged with argon and stored over molecular sieves 3 Å prior to use. The infrared spectra were measured on solid samples using a Perkin Elmer Spectrum 100 Fourier Transform infrared spectrometer in the range of 4000–500 cm^{-1}. Elemental analyses were carried out by the Analytical Department service at the Institute of Problems of Chemical Physics RAS using a vario MICRO cube (Elementar Analysensysteme GmbH) equipment.

2.1. Synthesis and characterization

$H_2DAPMBH$ (H_2L^{OCH3}) and H_2DAPBH (H_2L) ligands were prepared in a ketone-hydrazine condensation reaction between one equivalent of 2,6-diacetylpyridine and two equivalents of 4-methoxybenzoylhydrazine or benzoylhydrazine, respectively in 96% ethanol according to previously reported procedure [40,44]. The yields were more than 90% for both ligands.

H_2L^{OCH3}. Anal. Calc. for $C_{25}H_{25}N_5O_4$ (M.W.: 459 g mol^{-1}) C, 65.35; H, 5.48; N, 15.24%. Found: C, 65.62; H, 5.71; N, 15.35%. FT-IR ν_{max}/cm^{-1}: 3411 m, 3218 m, 2296 m, 1646 s, 1606 s, 1580 m, 1547 s, 1502vs, 1455 m, 1365 m, 1285 s, 1250vs, 1176vs, 1145 m, 1120 m, 1025 s, 919 m, 834vs, 758 m.

H_2L. Anal. Calc. for $C_{23}H_{21}N_5O_2$ (M.W.: 399 g mol^{-1}) C, 69.16; H, 5.30; N, 17.53%. Found: C, 69.25; H, 5.35; N, 17.49%. FT-IR ν_{max}/cm^{-1}: 3277 m, 1660vs, 1603 m, 1580 m, 1524vs, 1491 m, 1450 s, 1372 m, 1342 m, 1271vs, 1188 m, 1160 m, 1077 m, 917 s, 812 s, 708vs.

$[Cr(HL^{OCH3})Cl_2]\cdot 4CHCl_3$ (1). Compound **1** in the form of light brown block crystals suitable for X-ray diffraction analysis was obtained by recrystallization of **1a** from chloroform.

$[Cr(HL^{OCH3})Cl_2]\cdot CH_3OH$ (1a). To a suspension of H_2L^{OCH3} (0.65 mmol, 300 mg) in absolute methanol (19 ml) in Ar atmosphere solid $CrCl_2\cdot 4H_2O$ (127 mg, 0.65 mmol) was added while stirring. A green–brown mixture was stirred and heated at 60 °C for 1.5 h. The ligand was slowly dissolving during this time. Some yellow–brown solid developed after 30 min under stirring. The reaction mixture was stirred at 60 °C for additional 1 h to complete the reaction. After cooling to room temperature, the resulting yellow–brown precipitate was collected by filtration, washed with absolute CH_3OH, diethyl ether, and dried under vacuum. Yield: 16% (60 mg). Anal. Calc. for $CrC_{26}H_{28}N_5O_5Cl_2$ (M.W.: 613 g mol^{-1}) C, 50.91; H, 4.60; N, 11.42%. Found: C, 51.00; H, 4.75; N, 11.14%. FT-IR (solid) ν_{max}/cm^{-1}: 682 m, 744vs, 761vs, 804 m, 849vs, 1021 s, 1051 m, 1171vs, 1259vs, 1291 m, 1309 m, 1380vs, 1439 m, 1499 s, 1602vs, 1626 m, 2995 m, 3132 m. Carrying out the reaction under similar conditions, but in acetonitrile, leads to product $[Cr(HL^{OCH3})Cl_2]\cdot CH_3CN$ (1b) with a yield of about 80%. Anal. Calc. for $CrC_{27}H_{27}N_6O_4Cl_2$ (M.W.: 622 g mol^{-1}) C, 52.09; H, 4.37; N, 13.50%. Found: C, 52.55; H, 4.81; N, 13.40%. FT-IR (solid) ν_{max}/cm^{-1}: 682 m, 698 m, 762 s, 807 m, 848 s, 860 m, 1022 m, 1054 m, 1175vs, 1246 s, 1254 s, 1322 m, 1378vs, 1497 s, 1600 s.

$[Cr(HL^{OCH3})(H_2O)Cl]PF_6\cdot CH_3OH$ (2). All manipulations were performed in an inert atmosphere. $CrCl_2$ $4H_2O$ (53 mg, 0.27 mmol) was dissolved in 5 ml of 1 N aqueous HCl. This solution was added dropwise to a suspension of the ligand H_2L^{OCH3} in 10 ml of CH_3OH. The mixture was stirred for 1 h. Complete dissolution of the ligand and the formation

of a homogeneous green–brown solution occurred. The addition of excess of NH_4PF_6 to the cooled, filtered solution followed by slow evaporation over 2 weeks gave light brown crystals of **2.** (90 mg, yield 45%). The complex was identified by X-ray diffraction analysis.

[Cr(HL)(H_2O)Cl] ClO_4·0.25H_2O (3). To a mixture of H_2L (184 mg, 0.45 mmol) and $LiClO_4$ (190 mg ,1.78 mmol) in 17 ml of C_2H_5OH under Ar atmosphere solid $CrCl_2$ 4H_2O (90 mg, 0.46 mmol) was added while stirring. The green–brown mixture was stirred at 60 °C for 1 h, then cooled to r.t. and filtered. Light brown block crystals **3** suitable for single-crystal X-ray diffraction were obtained by slow evaporation of the filtrate after several days. Yield: 40% (112 mg). Anal. Calc. for $CrC_{23}H_{26}N_5O_7Cl_2$ (M.W.: 607 g mol^{-1}) C, 45.48; H, 4.31; N, 11.53%. Found: C, 45.91; H, 4.05; N, 11.75%. FT-IR (solid) ν_{max}/cm^{-1}: 697 s, 712vs, 811 m, 1051vs, 1099vs, 1132 s, 1169 s, 1273 m, 1300 s, 1392vs, 1425 m, 1500 s, 1526 s, 1572 m, 1600 m, 3256w, 3615w.

[Cr(HL^{OCH3})(H_2O)$_2$] (NO_3)$_2$·H_2O·C_2H_5OH (4). Complex **4** was prepared from Cr^{III} nitrate according to the literature method [25]. Yield: 45%. Anal. Calc. for $CrC_{27}H_{36}N_7O_{14}$ (M.W.: 734 g mol^{-1}) C, 44.14; H, 4.94; N, 13.35%. Found: 44.51; H, 5.25; N, 13.75%. FT-IR (solid) ν_{max}/cm^{-1}: 2958vs, 2904 s, 2867 s, 1606vs, 1557vs, 1529vs, 1494vs, 1386vs, 1315vs, 1269 s, 1190 m, 1166 m, 848 m, 682 m.

[Cr(L^{OCH3})(CH_3OH)(OCH_3)] ·CH_3OH (5). Complex **1a** (350 mg, 0.57 mmol) was added to 22 ml of CH_3OH. To this suspension the solution of $NaOCH_3$ in CH_3OH (0.44 M, 3.9 ml, 92 mg, 1.7 mmol) was added. The mixture was stirred for 10 min. The green–brown solid dissolved during this time and the color of the resulting solution turned red-brown. The reaction mixture was filtered and the filtrate was allowed to crystallize at r. t. After 10 days the red-brown crystalline solid (suitable for X-ray diffraction analysis) was separated from the mother liquor, washed with CH_3OH (5 ml), Et_2O (5 ml) and dried in vacuum to give **5.** Yield: 61% (210 mg). Anal. Calc. for $C_{28}H_{34}N_5O_7Cr$ (M.W.: 604.6 g mol^{-1}) C, 55.62; H, 5.67; N, 11.58%. Found: C, 55.31; H, 5.81; N, 11.62%. FT-IR (solid sample) ν, cm^{-1}: 2930 m, 1607 m, 1583 m, 1505 s, 1379vs, 1307 m, 1256 s, 1170 s, 1029vs, 994 m, 908 m, 842 s, 814 m, 761 s.

[Cr(HL^{OCH3})(NCS)$_2$] ·1.5H_2O (6). Complex **1a** (150 mg, 0.24 mmol) was added to 20 ml of CH_3OH. The mixture was stirred for 10 min., followed by the addition of the ethanol solution of NH_4NCS (90 mg, ~ 1 mmol in 8 ml EtOH). The resulting solution continued to stir at 50 °C for 1 h. The precipitate of **6** developed during the first 10 min. The green–brown mixture was cooled to r.t., and filtrated. The crystalline solid obtained was washed with Et_2O (2x5 ml) and dried in vacuum. Yield: 71% (111 mg). Anal. Calc. for $CrC_{27}H_{25}N_7O_5S_2$ (M.W.: 652 g mol^{-1}) C, 49.69; H, 3.91; N, 15.03; S, 9.82%. Found: C, 51.04; H, 4.35; N, 14.84; S, 9.35%. FT-IR (solid) ν_{max}/cm^{-1}: 761 s, 805 m, 844 s, 1024 m, 1051 m, 1171vs, 1255vs, 1301 m, 1383vs, 1493 s, 1561 m, 1603vs, 2064vs, 3075w, 3509w. Single crystals of **6** suitable for X-ray diffraction analysis were obtained by slow evaporation of mother liquor.

[Cr(HL^{OCH3})(N_3)$_2$] ·xH_2O (7, x = 0.2, 8, x = 0, 9, x = 0). To a methanol solution of NaN_3 (56 mg, 0.86 mmol in 16 ml) was added solid complex **1a** (50 mg, 0.082 mmol). The mixture was stirred at 60 °C for approximately 10 min. Then the hot cloudy mixture was filtered and left for crystallization under slow evaporation. After storing overnight at the room temperature, black crystals appeared, the color of the solution became pale yellow. The crystalline black solid was separated from solution by decantation, washed with CH_3OH (1.5 ml) and Et_2O (2 ml), dried under weak stream of Ar for 5 min. Yield: 67% (33 mg). Anal. Calc. for $C_{25}H_{24}N_{11}O_4Cr$ (M.W.: 604 g mol^{-1}) C, 50.51; H, 4.07; N, 25.92%. Found: C, 49.95; H, 4.36; N, 25.51%. FT-IR (solid sample) ν, cm^{-1}: 761 s, 844 m, 1024 s, 1168vs, 1252vs, 1308 m, 1338 m, 1381vs, 1508 m, 1559 m, 1607 s, 2059vs. In this reaction under an excess of NaN_3 from 2.5 to 10, three phases, (**7**, **8**, **9**) of the complex [Cr(HL^{OCH3})(N_3)$_2$]·xH_2O (**7**, x = 0.2, **8**, x = 0, **9**, x = 0) are formed in the same batch, which were identified by single crystal X-ray diffraction analysis (see crystal structure determination).

[Cr(L^{OCH3})(N_3)$_2$] [Na(CH_3OH)$_2$] ·2CH_3OH (10). To a solution of NaN_3 in absolute methanol (360 mg, 5.5 mmol of NaN_3 in 20 ml of CH_3OH) a portion of solid **1a** (60 mg, or 0.1 mmol) was added while stirring and the reaction mixture was stirred at 40 °C for 15 min. The formation of a homogeneous green–brown solution was observed. The reaction solution was cooled to r. t., filtered through a fritted glass filter and left for crystallization at room temperature. After a few hours, the formation of plate-shaped golden-brown crystals occurred. After this, the solvent was decanted, and the crystalline precipitate was washed with diethyl ether (2x3 ml) and dried in air. Upon drying, crystals of **10** easily lose crystallization alcohol. To carry out X-ray diffraction, the crystal was quickly removed from the mother liquor and immediately placed at a low temperature (200–250 K nitrogen stream, see Crystal structure determination section). Elemental analysis corresponds to a complex **10** without 2 CH_3OH solvate molecules. Yield: 67% (45 mg). Anal. Calc. for $CrNaC_{27}H_{31}N_{11}O_6$ (M.W.: 680 g mol^{-1}) C, 47.65; H, 4.59; N, 22.64%. Found: C, 47.41; H, 4.13; N, 22.84%. FT-IR (solid) ν_{max}/cm^{-1}: 765 s, 804 m, 849 s, 906 m, 1023vs, 1051 s, 1006 m, 1138 m, 1167vs, 1175vs, 1254vs, 1376vs, 1407 m, 1505 s, 1585 m, 1607 m, 2072vs, 2090vs, 2837 m, 3075 m, 3307w.

[Cr(L^{OCH3})(CN)$_2$] [Na(H_2O)(C_2H_5OH)] (11). A sample of complex **1a** (60 mg, or 0.1 mmol) was added to 15 ml of absolute methanol, and a solid sample of NaCN·2H_2O salt (40 mg, 0.47 mmol) was added to this suspension with stirring using a magnetic stirrer. The reaction mixture was stirred at 60 °C for 2 h. During this time, a complete dissolution of the complex observed followed the formation of a homogeneous red-brown color solution. The reaction mixture was cooled to room temperature, concentrated to about 5 ml by pumping out the solvent *in vacuo*. After this, a fine-crystalline orange precipitate developed. The precipitate was dissolved in ethanol, filtered through a glass filter and left at r. t. for slow evaporation. After some days, the formation of rhombus-shaped bright red crystals of **11** occurred. The mother liquor was decanted from the crystals; the precipitate was washed with diethyl ether (2x3 ml) and dried in air. Yield: 40% (26 mg). Anal. Calc. for $CrNaC_{29}H_{31}N_7O_6$ (M.W.: 648 g mol^{-1}) C, 50.91; H, 4.60; N, 11.42%. Found: C, 53.45; H, 4.93; N, 14.85%. FT-IR (solid) ν_{max}/cm^{-1}: 755 s, 840 m, 1055 s, 1173vs, 1244 s, 1369vs, 1505 s, 1591 m, 1604 s, 2137 m, 2943 m, 3230 m, 3406w.

2.2. Crystal structure determination

X-ray diffraction data were collected on an APEX II DUO CCD diffractometer (for **1**) and on an Oxford Diffraction Gemini-R CCD diffractometer (for **2**–**11**) [λ(MoKα) = 0.71073 Å, graphite monochromator, ω-scans]. Crystals **7**–**9** were found in the same dried batch; other single crystals were taken from mother liquid using a nylon loop with paratone oil and immediately transferred into cold (200–250 K) nitrogen stream of the diffractometer. All the transfer process took no more than 5–7 s to prevent solvent loss and to preserve diffraction quality of the crystals. Then crystals were cooled down to 120–150 K to collect the full set of data. Data reduction with empirical absorption correction of experimental intensities (Scale3AbsPack program) was made with the CrysAlisPro software [45]. The structures were solved by a direct method using SHELXS [46] or by a charge-flipping algorithm using Superflip [47] and refined by a full-matrix least squares method using SHELX-2016 program. All non-hydrogen atoms were refined anysotropically. The positions of H atoms were calculated geometrically and refined in a riding model with isotropic displacement parameters depending on U_{eq} of connected atom. Torsion angles for methyl and hydroxyl groups were refined using HFIX 137 and HFIX 147, respectively. N—H bonds were refined without restraints (except for DFIX in **2** and **7**). H atoms in water were found from difference Fourier map and refined with bond length restraints (SADI or DFIX). For disordered solvate water molecules with occupancy of 0.5 or less (in **3**, **6**, **7**) hydrogen atoms were not localized but included into compound formula.

In all the structures **1**–**11** the Cr complex is in a general position, i.e. its molecular geometry is not restricted by the crystal symmetry.

Position disorder was found in the structures **2** (PF_6^- anion and MeOH solvent), **3** (ClO_4^- and H_2O), **6** (central part of Cr^{III} complex, one NCS ligand and H_2O), **7** (one N_3 ligand), **8** (one N_3 ligand and one MeOPh-moiety of HL^{OCH3}). Non-merohedrally twinned structure **7** (twinning by a 180° rotation about c^*) was refined using HKLF5 data with twin fraction of 0.2155(8). Crystallographic data for all the complexes are listed in Table 1.

Crystallographic data for the structures reported in this paper have been deposited to the Cambridge Crystallographic Data Centre. These data can be obtained free of charge from The Cambridge Crystallographic Data via www.ccdc.cam.ac.uk/data_request/cif.

2.3. Magnetic measurements

Magnetic susceptibility measurements on complex **1** were carried out using Physical Properties Measurements System PPMS-9 (Quantum Design) in the temperature range of $T = 2$–300 K under magnetic field up to $B = 9$ T. The samples in polycrystalline (powder) form were loaded into an insulating capsule. The experimental data were corrected for the sample holder. The diamagnetic contribution from the ligand was calculated using Pascal's constants.

3. Results and discussion

3.1. Synthesis of 1–11

Ten of the eleven compounds described in this work were obtained using the pentadentate ligand with the $[N_3O_2]$ binding node, 2,6-diacetylpyridine bis(4-methoxybenzoylhydrazone), H_2L^{OCH3}, that was synthesized by us via ketone-hydrazine condensation reaction between 2,6-diacetylpyridine and 4-methoxy-benzoylhydrazine in 96% ethanol similarly to previously reported procedure [40,44]. The compound was

Table 1
Crystallographic data and refinement parameters for **1**–**11**.

	1	**2**	**3**	**4**	**5**	**6**
Chemical formula	$C_{29}H_{28}Cl_{14}CrN_5O_4$	$C_{26}H_{30}ClCrF_6N_5O_6P$	$C_{23}H_{22.5}Cl_2CrN_5O_{7.25}$	$C_{27}H_{36}CrN_7O_{14}$	$C_{28}H_{34}CrN_5O_7$	$C_{27}H_{27}CrN_7O_{5.5}S_2$
M, g/mol	1058.86	740.97	607.86	734.63	604.6	653.67
Crystal system	triclinic	monoclinic	triclinic	triclinic	monoclinic	monoclinic
Space group	P-1	$C2/c$	P-1	P-1	$P2_1/c$	$C2/c$
T, K	120	150	150	150	150	150
a, Å	11.021(2)	23.6793(3)	10.6884(1)	8.6705(1)	18.0177(4)	21.8426(4)
b, Å	13.694(3)	12.0298(2)	10.7350(1)	13.4643(2)	7.4036(2)	14.4563(2)
c, Å	15.179(3)	22.7889(3)	11.9854(2)	13.7681(2)	21.7447(7)	19.9308(5)
α, °	91.83(3)	90	107.402(1)	90.272(1)	90	90
β, °	103.76(3)	90.052(1)	96.942(1)	90.923(1)	91.852(3)	99.837(2)
γ, °	108.40(3)	90	101.0624(9)	95.971(1)	90	90
V, Å^3	2097.0(8)	6491.6(1)	1264.33(3)	1598.36(4)	2899.1(1)	6200.9(2)
Z	4	8	2	2	4	8
ρ_{calcd}, g/cm^3	1.677	1.516	1.597	1.526	1.385	1.400
μ, mm^{-1}	1.207	0.565	0.719	0.439	0.448	0.553
Θ range, °	1.58–29.00	1.90–29.00	2.05–29.50	2.11–25.25	2.16–29.00	2.07–29.00
N_{total}	25,626	19,108	25,935	16,756	18,086	21,270
N_{unique}	11,139	9019	7337	8146	8039	8784
R_{int}	0.0230	0.0127	0.0170	0.0147	0.0222	0.0205
N_{refl} ($I \geq 2\sigma(I)$)	9493	7743	6521	7284	6186	6298
$N_{parameters}$	482	503	408	469	379	457
R_1, wR_2 ($I \geq 2\sigma(I)$)	0.0376, 0.1267	0.0532, 0.1343	0.0342, 0.0891	0.0384, 0.1017	0.0422, 0.0900	0.0656, 0.1769
R_1, wR_2 (all data)	0.0458, 0.1369	0.0621, 0.1417	0.0400, 0.0932	0.0440, 0.1063	0.0624, 0.1007	0.0921, 0.1993
$\Delta\rho_{min}/\Delta\rho_{max}$, e/Å^3	1.74 / −1.14	1.13 / −1.05	0.62 / −0.75	0.78 / −0.47	0.58 / −0.43	1.08 / −0.74
GOF	1.027	1.000	1.000	1.001	1.000	1.001
CCDC number	1850320	2013957	2013958	2013959	2013960	2013961

	7	**8**	**9**	**10**	**11**
Chemical formula	$C_{25}H_{24.4}CrN_{11}O_{4.2}$	$C_{25}H_{24}CrN_{11}O_4$	$C_{25}H_{24}CrN_{11}O_4$	$C_{29}H_{39}CrN_{11}NaO_8$	$C_{29}H_{31}CrN_7NaO_6$
M, g/mol	598.15	594.55	594.55	744.7	648.6
Crystal system	monoclinic	triclinic	monoclinic	monoclinic	triclinic
Space group	$P2_1/n$	P-1	$P2_1/c$	$P2_1/c$	P-1
T, K	150	150	150	150	150
a, Å	10.4048(1)	9.3767(3)	14.746(2)	16.5539(3)	10.3246(1)
b, Å	13.9974(2)	10.6915(3)	13.952(2)	8.2006(2)	12.4590(2)
c, Å	18.8722(2)	14.5124(8)	14.604(2)	26.4264(5)	13.3384(2)
α, °	90	102.116(4)	90	90	111.089(1)
β, °	95.2214(9)	107.086(4)	115.97(1)	99.724(2)	104.890(1)
γ, °	90	103.583(3)	90	90	93.537(1)
V, Å^3	2737.13(5)	1289.4(1)	2701.1(7)	3535.9(1)	1524.32(4)
Z	4	2	4	4	2
ρ_{calcd}, g/cm^3	1.452	1.531	1.462	1.399	1.413
μ, mm^{-1}	0.473	0.501	0.478	0.399	0.444
Θ range, °	1.81–29.00	2.05–29.25	2.12–27.00	2.50–28.75	1.78–29.00
N_{total}	27,276	21,109	14,797	21,805	19,480
N_{unique}	7883	11,458	5858	9595	8566
R_{int}	0.0163	0.0299	0.0588	0.0248	0.0162
N_{refl} ($I \geq 2\sigma(I)$)	6842	8031	3556	7707	7486
$N_{parameters}$	404	378	444	463	409
R_1, wR_2 ($I \geq 2\sigma(I)$)	0.0349, 0.0947	0.0584, 0.1644	0.0985, 0.2349	0.0429, 0.1081	0.0331, 0.0819
R_1, wR_2 (all data)	0.0416, 0.1002	0.0808, 0.1743	0.1530, 0.2645	0.0580, 0.1175	0.0404, 0.0865
$\Delta\rho_{min}/\Delta\rho_{max}$, e/Å^3	0.41 / −0.38	1.44 / −0.71	1.49 / −1.21	0.77 / −0.41	0.46 / −0.42
GOF	1.003	1.003	1.000	1.004	1.000
CCDC number	2013962	2013963	2013964	2013965	2013966

isolated in a solid state; its composition was confirmed by elemental analysis and IR spectra.

3.2. Synthesis of dichloride Cr^{III} complexes with H_2L^{OCH3} ligand.

In the beginning of this work we intended to prepare seven-coordinate chromium complexes in the oxidation states +II and +III, therefore we used simple salts of both bivalent and trivalent chromium $CrCl_2{\cdot}4H_2O$, $CrCl_3{\cdot}6H_2O$, $Cr(NO_3)_3{\cdot}6H_2O$.

We found that regardless of the metal oxidation state (+II or +III) in the starting compound as well as additional precautions (reaction in aprotic solvents, in an inert atmosphere and in the presence of a reducing agent, dithionite), Cr(III) complexes were always formed. Apparently, this is because the H_2L^{OCH3} ligand oxidizes Cr^{II} to Cr^{III}, which forms a complex of trivalent chromium stable under the reaction conditions.

The interaction of the $CrCl_2{\cdot}4H_2O$ salt with the H_2L^{OCH3} ligand in methyl alcohol in the absence of air oxygen leads to the formation and precipitation of a poorly soluble in methanol neutral complex $[Cr^{III}(HL^{OCH3})Cl_2]{\cdot}CH_3OH$ (**1a**). The yield of complex **1a** under these conditions does not exceed 20% for the taken $CrCl_2{\cdot}4H_2O$. The type of solvent greatly affects the yield of the reaction product. The interaction of $CrCl_2{\cdot}4H_2O$ with the H_2L^{OCH3} ligand in an aprotic solvent, for example, acetonitrile or chloroform, leads to the same complex, $[Cr^{III}(HL^{OCH3})Cl_2]{\cdot}$solv, but with a yield of up to 80%. We also found that if we use the $CrCl_3{\cdot}6H_2O$ salt as the source of chromium, then the reaction with H_2L^{OCH3} in methanol does not proceed at all, as is usually the case due to the high kinetic inertness of the $CrCl_3{\cdot}6H_2O$ aqua complex to substitution reactions [48]. However, in acetonitrile (or in a mixture of $CH_3OH + CH_3CN$) this reaction proceeds at a high rate and leads to the complex $[Cr^{III}(HL^{OCH3})Cl_2]{\cdot}CH_3CN$ (**1b**) with a very high yield (more than 80%). Preparation of single crystals of **1** required recrystallization of (**1a**) or (**1b**) from $CHCl_3$, while single crystals of all other complexes described below were obtained by slow evaporation of the filtered mother liquors.

Dichloride complexes of type **1**, $[Cr^{III}(HL^{OCH3})Cl_2]{\cdot}$solv, Fig. 1a, are neutral molecules with a pentadentate ligand in mono-deprotonated form $(HL^{OCH3})^{1-}$ as an equatorial ligand and two axial Cl^- ligands (see below for a detailed description of the structure).

In the course of the reaction of $CrCl_2{\cdot}4H_2O$ with H_2L^{OCH3} in CH_3OH, in addition to the neutral complex **1a** that is practically insoluble in methanol, a significant amount of the ionic complex $[Cr^{III}(HL^{OCH3})(H_2O)Cl]Cl$, readily soluble in CH_3OH is formed. The compound can be isolated in crystalline form by the addition of a large anion, for example, ClO_4^- or PF_6^-, to the reaction mixture, see, for example, complexes **2**, **3**, Fig. 1b and Figs. S3, S5. In these compounds, the Cr^{III} ion is part of the complex cation, and Cl^- and H_2O act as axial ligands.

In all the Cl^- containing complexes described above, the pentadentate ligand is in the monodeprotonated form $[HL^{OCH3}]^{1-}$. We note here that it was not possible to avoid deprotonation of the H_2L^{OCH3} ligand during the reactions and to obtain a Cr^{III} complex with the ligand in the neutral form $[H_2L^{OCH3}]^0$ even when carrying out the reaction in a strongly acidic medium in a mixture of $CH_3OH + H_2O + HCl$ (see, for example, complex **2** synthesis).

The use of chromium (III) nitrate instead of chloride allowed to obtain an ionic complex containing two water molecules as axial ligands, $[Cr^{III}(HL^{OCH3})(H_2O)_2](NO_3)_2$ (**4**), Fig. S6. Complexes of Cr(III) similar to **4**, i.e. containing no solvent molecules in the first coordination sphere, were obtained earlier with two other pentadentate ligands [25].

3.3. Replacement of axial Cl^- ligands in dichloride complexes by CH_3O^-, NCS^-, $(N_3)^-$, CN^-.

The axial chloride ligands in compounds **1**, **1a,b** can be easily replaced by several other mono-charged or neutral ligands while maintaining the overall geometry of the complex in the form of a pentagonal bipyramid. Preparation and some reactions of $[Cr^{III}(HL^{OCH3})$

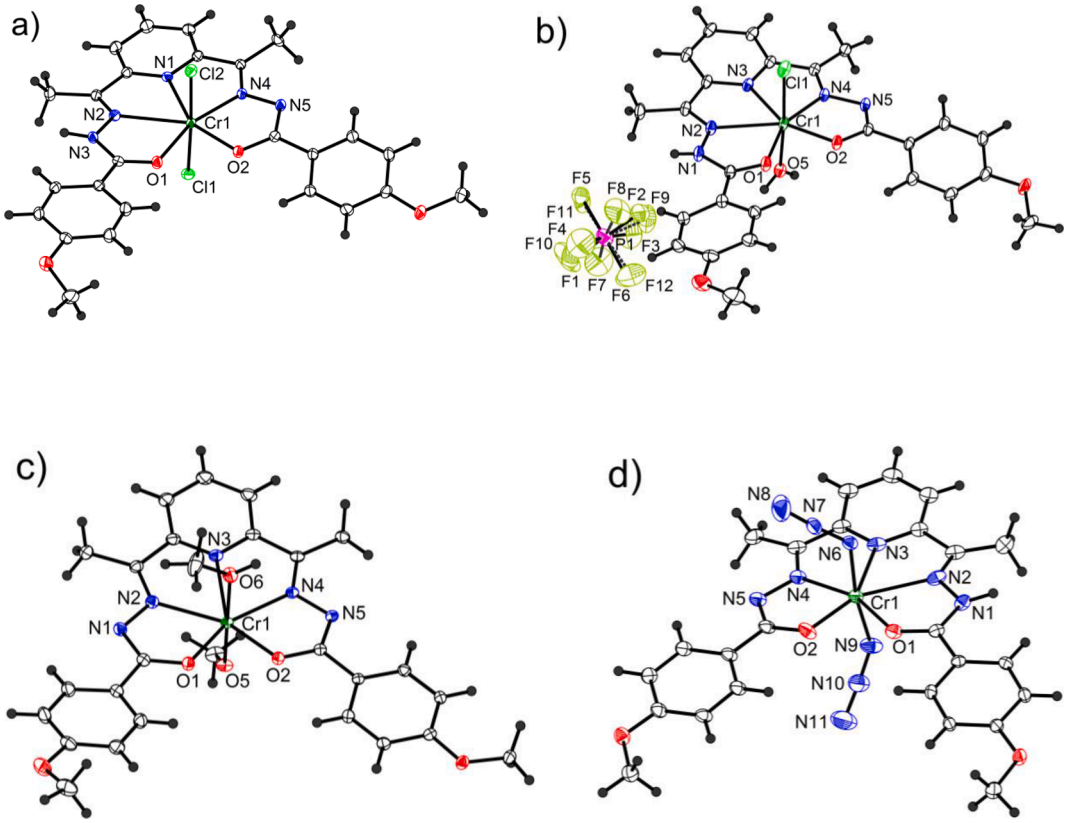

Fig. 1. Molecular structures of complexes **1** (a), **2** (b), **5** (c) and **8** (d) with partial atom numbering. Solvent molecules are omitted for clarity.

Cl_2] are summarized in Fig. 2.

In particular, the neutral complex [$Cr^{III}(L^{OCH3})(CH_3OH)(OCH_3)$]·$CH_3OH$ (**5**), Fig. 1c, S7 containing CH_3OH molecule and a methoxide group as apical ligands, is formed by adding stoichiometric amounts of sodium methoxide to a suspension of complex **1a** in methanol at room temperature. In the presence of $NaOCH_3$, **1a** dissolves in methanol and complex **5** crystallizes from the resulting orange homogeneous solution. $NaOCH_3$, being a strong base, leads not only to the replacement of axial Cl^- ligands with coordinated methoxide and methanol, but also to the complete deprotonation of the equatorial ligand. The molecules of complex **5** in the crystal are joined by strong hydrogen bonds, Fig. S8.

The reaction of the complex **1a** with ammonium thiocyanate in methanol leads to a simple replacement of Cl^- ligands with NCS^- groups and the formation of a neutral complex **6**, the structure of which is shown in Figs. S9, S10.

The axial chloride ligands in **1a** can also be easily replaced, for example, by $(N_3)^-$ zide ligand. Interestingly, depending on the ratio $(N_3)^-$/Cr, one can obtain either neutral pentagonal bipyramidal complex with terminal azide ligands in axial positions, or linear Cr-Na cluster with bridging azide ligands of various types. When the ratio of reagents NaN_3/Cr = 2.5 ÷ 10, three phases (**7**, **8**, **9**) of the complex [Cr(HL^{OCH3})$(N_3)_2$]·xH_2O (**7**, x = 0.2, **8**, x = 0, **9**, x = 0) are formed in the same synthesis, which were identified by single crystal X-ray diffraction analysis, Fig. 1d and S11-S15. The formation of a heterometallic Cr-Na complex [$Cr^{III}(L^{OCH3})(N_3)_2$][Na $(CH_3OH)_2$]·2CH_3OH (**10**) can be observed under the condition of a very large excess of sodium azide in the reaction medium (greater than 50 mol NaN_3 per mole of the chromium complex **1a**), Fig. 7, S16. In this compound, the equatorial ligand is in a doubly-deprotonated form $(L^{OCH3})^{2-}$. The complex **10** contains two types of bridging $(N_3)^-$ ligands: (*μ-1,3*-N_3) and (*μ-1,1*-N_3) between chromium and sodium atoms. This is just the second example, described in the literature, of a heterometallic complex containing Cr(III) and Na (I) ions connected by azide bridges. Synthesis and structure of the first azido bridged Cr-Na complex is reported in ref. [49].

The axial Cl- ligands in compound **1** can also be easily replaced by CN^- groups by reaction of **1** with sodium cyanide. In this case, the complete deprotonation of the equatorial ligand and the replacement of Cl^- axial ligands by CN^- groups are observed. As a result, an ionic complex **11** is formed, including the Na^+ cation, balancing the charge of the complex anion [$Cr^{III}(L^{OCH3})(CN)_2$]$^-$, Fig. S17. In the crystal, two anionic seven coordination Cr^{III} containing fragments are combined into dimers, Fig. 8.

Solid state FT-IR spectroscopic analysis of the complexes **1**–**11** showed the disappearance of characteristic strong ν (C═O) band of the free ligand and the appearance of a new band between 1365 and 1377 cm^{-1} confirming the complexation of the ligand [HL^{OCH3}]$^{1-}$ or [L^{OCH3}]$^{2-}$ with the metal [17,25], see for example the IR spectrum of complex **10**, Fig. S16. In addition, intense bands of axial ligands are observed, in particular, in complex **6** – very strong bands at 2064 cm^{-1} are due to ν (C═N) of the thiocyanate ligand [25,50], in complexes **7, 8, 9** – 2059 cm^{-1} (ν N_3 groups) [50], in complex **10** – two bands, 2072 and 2090 cm^{-1}, related to two types of bridging ligands - μ2 (1,1) and μ2 (1,3) $(N_3)^-$ [51], Fig. S18. In the FT-IR spectrum of complex **11** a medium band appears at 2137 cm^{-1} which is attributed to apical cyanide ligands [25].

3.4. Description of the structures

Some important structural parameters, bond lengths (Å) and angles (°), as well as hydrogen bond geometry for complexes **1**–**11** are collected in Tables S1–S21 (Supplementary data).

3.5. Neutral complexes (1, 5–9)

Five of the six charge-neutral heptacoordinated Cr^{III} complexes contain the monodeprotonated monoanionic [HL^{OCH3}] $^-$ ligand (**1**, **6**, **7**, **8**, **9**) and one more complex (**5**) contains doubly deprotonated dianionic [L^{OCH3}]$^{2-}$ ligand, as exemplified in Figs. 1, 2. In all the complexes, the central Cr^{III} ion is coordinated by three nitrogen and two oxygen atoms of the pentadentate ligand in the equatorial plane and by two apical ligands together forming a distorted pentagonal bipyramidal coordination polyhedron. In complexes with [HL^{OCH3}]$^-$, the apical ligands are two identical monocharged anions, Cl^- in **1**; NCS^- in **6** or N_3^- in **7**–**9**. Complex **5** with doubly deprotonated ligand [L^{OCH3}]$^{2-}$ contains one neutral methanol molecule and one charged methoxy group CH_3O^- in the apical positions.

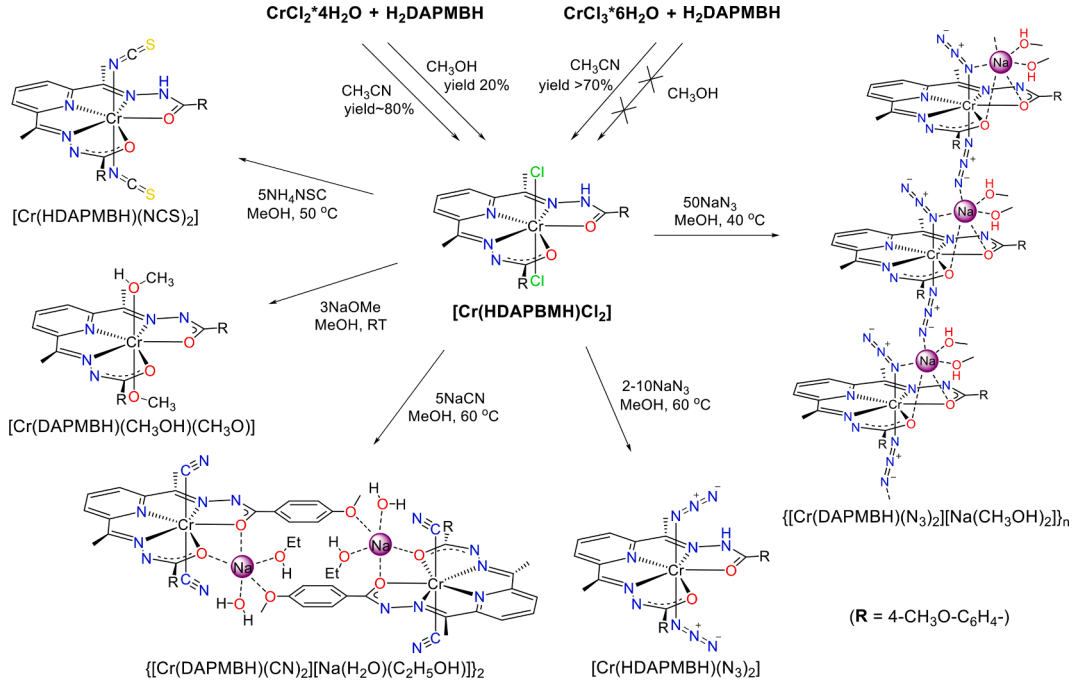

Fig. 2. General scheme for the synthesis of the Cr^{III} dichloride complex with the H_2DAPMBH ligand and the substitution reactions of axial Cl ligands.

Chromium complexes **1**, **6**, **7**, **8**, **9** with monodeprotonated $[HL^{OCH3}]^-$ ligand reveal pronounced distortion from the idealized C_{2v} symmetry, as can be seen from Fig. 3a and Tables 2 and 3, which compare atomic distances in the five-membered deprotonated (CrN_2CO) and protonated (CrN_2HCO) cyclic groups. Deprotonation of the hydrazide NH moieties in the pentadentate ligand is followed by changes in the bond lengths, namely, the C—N bonds are shorter and O—C bonds are longer in the deprotonated cycles, *R*(C—N) = 1.319–1.331 Å vs. *R*(C—N) = 1.341–1.360 Å and *R*(O—C) = 1.289–1.297 Å vs. *R*(O—C) = 1.241–1.253 Å in the deprotonated and protonated cycles, respectively, Tables 2 and 3 (compound **6** is missed in our comparative analysis because of the positional disorder of the central part of the Cr complex). On the other hand, our structural data for compounds **1**–**4**, **6**–**9** with monodeprotonated $[HL^{OCH3}]^-$ ligand show that deprotonation has considerably stronger impact on the Cr coordination bonds. In fact, both the Cr-O and Cr-N bonds are considerably shorter in the deprotonated cyclic group: *R*(Cr-O) = 1.926–1.952 Å in CrN_2CO cycles vs. 2.060–2.137 Å in CrN_2HCO and *R*(Cr-N) = 2.034–2.066 Å (CrN_2CO) vs. 2.414–2.452 Å (CrN_2HCO). The maximum difference in the Cr-N bond length reaches ca. 0.4 Å. Below we show that, apart from deprotonation, this distortion is caused by the strong first-order Jahn-Teller effect in the high-spin $3d^3$ system under the pentagonal bipyramidal ligand field (see below Figs. 9 and 10).

In all the compounds **1**, **5**–**9**, the Cr^{III} complexes enter as isolated molecular units which interact with each other only by hydrogen bonding and π-stacking. Most of the compounds contain H-bonded dimers, in which the metal complexes are linked by pair of equivalent hydrogen bonds from the NH donor to the acceptor atom (Cl, N) of the axial ligand (Fig. 4). In this interaction, half of the ligand of one complex is π-stacked with half of the ligand of another complex causing formation of the shortened C…C contacts as shown in Fig. 4. The Cr…Cr distances in the dimer range from 6.660 Å (in **8**) to 7.341 Å (in **1**). In **5**, in the absence of NH protons, infinite chains form along the *b* axis with hydrogen bonding between the axial ligands of neighboring complexes through the solvent methanol bridging molecules: CH_3OH_{ligand}…$CH_3OH_{solvent}$…$OCH_{3\,ligand}^-$, Fig. S8. In **6** the indirect intradimer hydrogen bonding is mediated through the bridging water molecules: $N\text{-}H_{HLOCH3}$…H_2O…S_{NCS}. Details of intermolecular interactions are given in the Supplementary information, Fig. S9, S10, Table S11.

3.6. Cationic complexes (2–4)

In compounds **2**–**4**, the chromium ion is incorporated into the complex cation. Cationic complexes were synthesized with monodeprotonated HL^{OCH3} (**2**, **4**) or HL (**3**) pentadentate equatorial ligand. Complexes **2** and **3** contain one neutral (H_2O) and one anionic (Cl^-) ligands in the apical positions and bear positive charge (+1) compensated by PF_6^- or ClO_4^- counter anions, respectively. In complex **4** both apical ligands are neutral water molecules; this cationic complex has a charge of +2 compensated by two NO_3^- counter anions. Molecular structure of the cationic Cr complexes, including bond lengths and angles, is very similar to the structure of the neutral complexes **1**, **5**–**9** described above. The Cr^{III} center is in the distorted pentagonal-bipyramidal coordination.

The structures **2** and **3** consist of infinite chains in which Cr complexes are linked by pairs of hydrogen bonds: N—H…Cl from one side and O—H…N from the other side (Fig. 5). Hydrogen bond geometry in **2**/**3**: H…Cl distances 2.41/2.79 Å, N—H…Cl angles 165.7/151.6°; H…N 1.90/1.95 Å, O—H…N 169.5/174.1 °. Distances between the Cr centers along the chain in **2**/**3** are 7.050/7.335 Å for N—H…Cl linkage and 6.264/6.191 Å for O—H…N linkage. A π-stacking interaction between two half-ligands is also observed along the chain. In **2** the chains are packed into layers in the *ab* plane. In the neighboring layers, chain directions are not parallel, [1 1 0] or [1 –10]. The anions and solvent molecules locate between the layers. In **3** all the chains run along the [0 1 1] direction, forming the layers in the (0 1–1) plane.

In **4** the NH function is deactivated by a formation of hydrogen bond with solvate ethanol molecules. Dimeric structure is stabilized by pair of O—H…O hydrogen bonds between H_2O axial ligand and oxygen atom of the pentadentate ligand coordinated to Cr (Fig. 6). H…O distance is 1.87 Å, O—H…O angle is 174.2 °. The Cr…Cr distance in the dimer is very short, 4.979 Å. Other protons of water ligands are engaged into strong hydrogen bonding with surrounding NO_3^- anions with H…O distances in the range of 1.81–1.84 Å.

3.7. Anionic complexes (10–11)

Anionic complexes **10**–**11** contain dianionic $[L^{OCH3}]^{2-}$ ligands and two N_3^- or CN^- anions in apical positions. The negative electric charge (-1) of the metal complex is compensated by Na^+ cation. The bond lengths in complexes with doubly deprotonated ligand (**5**, **10**, **11**) differ from those in complexes with monodeprotonated ligand (Fig. 3b and Table 4).

Given the same nature of the deprotonated five-membered CrN_2CO cyclic groups in complexes with monodeprotonated and doubly deprotonated ligands (Fig. 3), it is reasonable to expect that bond lengths in two deprotonated CrN_2CO cycles of the CrL^{OCH3} moiety should be close to those in the similar deprotonated cycle of the $CrHL^{OCH3}$ moiety (Table 2). However, our data indicate that the Cr-N and Cr-O bond lengths in $Cr[L^{OCH3}]^{2-}$ (*R*(Cr-N) = 2.11–2.29 Å and *R*(Cr-O) = 1.97–2.02 Å, Table 4) are longer than in the deprotonated cycle of Cr $[HL^{OCH3}]^-$ (in fact, they lie in between the ranges for protonated and deprotonated cycles of the latter, see Tables 2 and 3). Besides, in doubly deprotonated complexes with $[L^{OCH3}]^{2-}$, the Cr-N bond to the N atom of pyridine is longer by ~ 0.1 Å (2.367–2.423 Å) than in monodeprotonated complexes with $[HL^{OCH3}]^-$ (2.242–2.300 Å). At the same

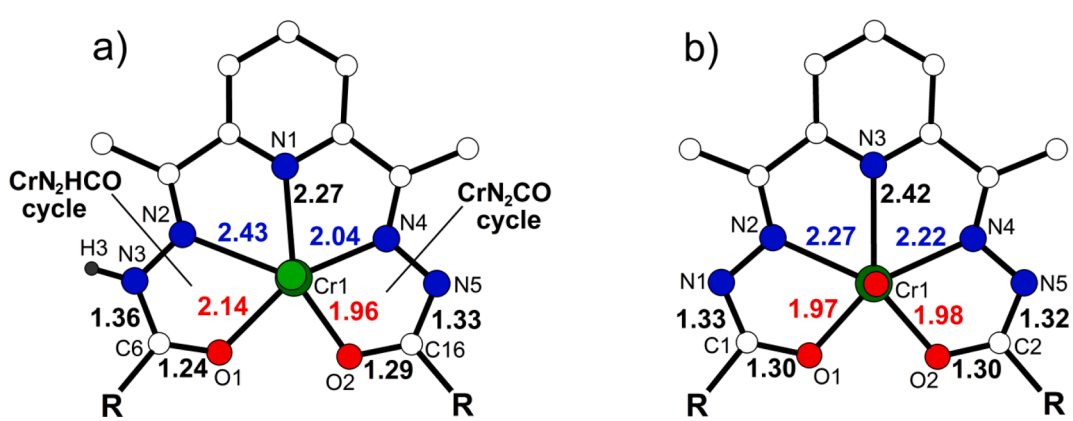

Fig. 3. Comparison of bond length values (Å) in the Cr complexes with $[HL^{OCH3}]^-$ (a, complex **1**) and $[L^{OCH3}]^{2-}$ (b, complex **5**) ligands.

Table 2
Bond lengths (Å) in the deprotonated CrN_2CO cycles of Cr(III) complexes with HL and HL^{OCH3} mono-charged ligands.

	1	**2**	**3**	**4**	**6**(a)*	**6**(b)*	**7**	**8**	**9**
Complex charge	0	1+	1+	2+	0	0	0	0	0
Ligand charge	1-	1-	1-	1-	1-	1-	1-	1-	1-
Cr-N	2.034(2)	2.053(2)	2.037(1)	2.026(1)	2.078(4)	2.038(3)	2.041(1)	2.066(2)	2.049(5)
Cr-O	1.952(1)	1.951(1)	1.935(1)	1.968(1)	1.92(1)	1.97(2)	1.948(1)	1.926(2)	1.946(4)
O—C	1.289(2)	1.286(2)	1.288(2)	1.311(2)	1.31(1)	1.30(2)	1.297(1)	1.296(3)	1.289(6)
C—N	1.329(2)	1.331(3)	1.329(2)	1.316(2)	1.324(3)	1.342(3)	1.319(2)	1.319(3)	1.331(7)

* **6**(a) and **6**(b) are two positions of the disordered $CrHL^{OCH3}$ in **6**

Table 3
Bond lengths (Å) in the protonated CrN_2HCO cycles of Cr(III) complexes with HL and HL^{OCH3} mono-charged ligands.

	1	**2**	**3**	**4**	**6**(a)*	**6**(b)*	**7**	**8**	**9**
Complex charge	0	1+	1+	2+	0	0	0	0	0
Ligand charge	1-	1-	1-	1-	1-	1-	1-	1-	1-
Cr-N	2.420(2)	2.392(2)	2.409(1)	2.441(1)	2.394(3)	2.331(5)	2.452(1)	2.414(3)	2.437(5)
Cr-O	2.137(2)	2.085(1)	2.086(1)	2.078(1)	2.08(1)	2.19(2)	2.088(1)	2.060(2)	2.077(4)
O—C	1.241(2)	1.245(2)	1.242(2)	1.257(2)	1.26(1)	1.23(2)	1.252(1)	1.253(3)	1.244(6)
C—N	1.357(2)	1.353(3)	1.350(2)	1.354(2)	1.342(3)	1.324(3)	1.360(2)	1.359(4)	1.341(7)

* **6**(a) and **6**(b) are two positions of the disordered $CrHL^{OCH3}$ in **6**

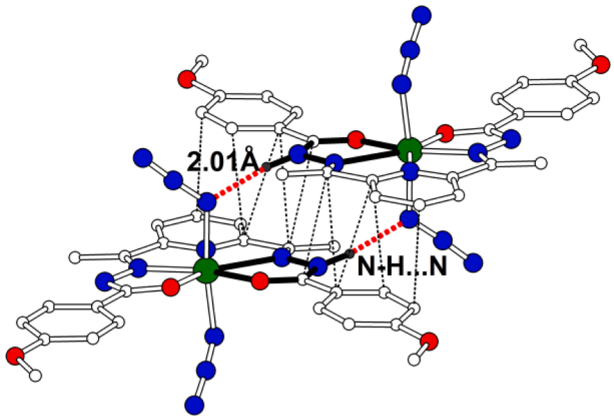

Fig. 4. Hydrogen-bonded dimer in **7**. N—H…N bonds are shown by thick red dashed lines. Shortened C…C contacts in π-stacking interaction of 3.347–3.504 (5) Å are marked by thin black dotted lines. The Cr…Cr intradimer distance is 6.786(1) Å.

time, the C—O and C—N bonds have similar lengths in the CrN_2CO cycles of the complexes with both mono- and doubly deprotonated ligands, i.e. pronounced difference is observed only within the $Cr^{III}N_3O_2$ pentagon.

These structural features are well consistent with the strong Jahn-Teller (JT) effect in high-spin pentagonal-bipyramidal Cr^{III} complexes. An important point is that the deprotonation of the equatorial ligand

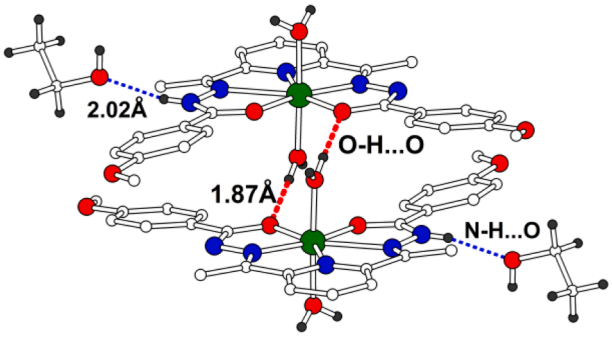

Fig. 6. Hydrogen-bonded dimer in **4**.

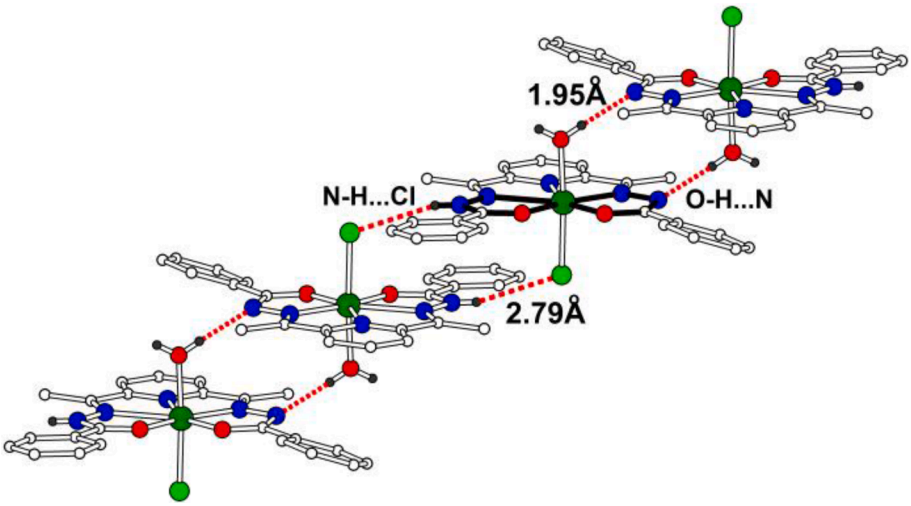

Fig. 5. Hydrogen-bonded chain in the structure **3**.

Table 4
Bond lengths (Å) in the deprotonated CrN_2CO cycles of Cr(III) complexes with L^{OCH3} double-charged ligand.

	5	5	10	10	11	11
Complex charge	0	0	1-	1-	1-	1-
Ligand charge	2-	2-	2-	2-	2-	2-
Cr-N	2.266 (1)	2.218 (1)	2.114 (1)	2.291 (1)	2.183 (1)	2.209 (1)
Cr-O	1.970 (1)	1.978 (1)	1.970 (1)	2.015 (1)	1.965 (1)	1.983 (1)
O—C	1.296 (2)	1.295 (2)	1.302 (2)	1.288 (2)	1.304 (1)	1.301 (1)
C—N	1.327 (2)	1.322 (2)	1.310 (2)	1.320 (2)	1.311 (2)	1.313 (2)

causes a reversal of the direction of the JT distortion associated with the in-plane shift of Cr atom from the central position in the $Cr^{III}N_3O_2$ pentagon resulting in the appearance of one long Cr-N bond (~2.4 Å). More specifically, the long Cr-N bond switches from the side N atom of the hydrazide group to the N atom of pyridine upon passing from mono- to doubly deprotonated ligands (see Figs. 9 and 10 in the next Section).

The $Cr(L^{OCH3})$ moieties in the structure **10** are connected into 1D coordination polymer along *b* through azide bridges and Na^+ cations (Fig. 7). The bridging azide ligands link Cr and Na centers in an end-to-end (*μ-1,3*-N_3) and an end-on (*μ-1,1*-N_3) bonded fashion. The Cr-N and Na-N distances are 2.031 and 2.366 Å for *μ-1,3*-N_3, 2.025 and 2.590 Å for *μ-1,1*-N_3, respectively. The latter interaction is strengthened by two oxygen atoms of the pentadentate ligand which are also binded to the Na^+ cation, Cr-O bond lengths are 2.016 and 1.970 Å, Na-O distances are 2.415 and 2.508 Å. In addition, two methanol molecules are coordinated to Na^+ (Na-O 2.334 and 2.351 Å), one of which forming hydrogen bond of O—H…N type to the next CrL^{OCH3} moiety in the chain (H…N 2.10 Å, O—H…N angle 174.4 °). Cr…Cr distances are 8.201 Å along the chain and 8.038 Å between the π-stacked pentadentate ligands from the neighboring chains.

In **11** the dimeric unit is formed by pair of $[Cr(L^{OCH3})(CN)_2]^-$ anionic complexes linked via sodium cations (Fig. 8). Two oxygen atoms of pentadentate ligand of one Cr complex and oxygen atom of the terminal methoxy group of another complex are coordinated to the same Na^+ ion. Cr-O distances are 2.388 and 2.477 Å for the former and 2.592 Å for the latter interaction. One ethanol and one H_2O molecules are bonded to Na^+. They form O—H…N hydrogen bonds to CN axial ligands of the Cr complexes outside of the dimer, H…N distance and O—H…N angle are 1.92 Å and 167.3° for C_2H_5OH, 2.10 Å and 169.4° for H_2O. The shortest Cr…Cr distance in the structure **11** of 8.146 Å is found between the complexes linked through Na^+ and C_2H_5OH. The distance between the Cr centers in the dimeric unit is 12.427 Å.

4. Origin of the in-plane distortions in PBP Cr^{III} complexes: Manifestation of the first-order Jahn-Teller effect

All heptacoordinated Cr^{III} complexes **1**–**11** invariably show strong in-plane distortions resulting from the shift of Cr atom from the central position in the CrN_3O_2 pentagon followed by formation of one long Cr–N bond (Fig. 3 and Tables 2,3). The same is also true for the closely related complexes $[Cr^{III}(L^{N3O2R})X_2]$ (where L^{N3O2R} is a N_3O_2 Schiff-base ligand and X = H_2O, CN, NCS are the apical ligands) previously reported in ref. [25] (compounds 1–5, crystal structures CCDC 1561578–1561582). The fundamental reason behind these distortions is the strong first-order Jahn-Teller (JT) effect; its origin for high-spin ($S = 3/2$) PBP $Cr^{III}(3d^3)$ complexes with the central planar $Cr^{III}N_3O_2$ pentagon is illustrated in Fig. 9. In the regular PBP coordination of $Cr^{III}(3d^3)$ ion (D_{5h} symmetry), two electrons with parallel spins occupy the two lowest 3d-orbitals *xz* and *yz* and the third electron occupies one of the two excited degenerate (symmetry-related) orbitals *xy* and x^2-y^2 (Fig. 9a) resulting in double orbital degeneracy of the ground state, which is represented by two many-electron wave functions *det*||*xz*↑, *yz*↑, *xy*↑|| and *det*||*xz*↑, *yz*↑, x^2–y^2↑||. Therefore, high-spin PBP complexes of Cr^{III} undergo JT distortions, which lower the energy of one of the degenerate orbitals (*xy* and x^2-y^2) and increase the energy of the other orbital, thereby leading to a total energy gain of ΔE_{JT} (Fig. 9b). In-plane displacements of the Cr^{III} ion in the CrN_3O_2 pentagon cause especially strong energy splitting of the excited orbitals *xy* and x^2-y^2 because they interact in the σ-bonding mode with the valent orbitals of the N and O atoms in the equatorial plane N_3O_2 (Fig. 9b). By contrast, the π-bonding orbitals *xz* and *yz* undergo weak splitting upon distortions, which account for a small distortion of the N_3O_2 pentagon in the low-spin Mo(III) complex $[Mo^{III}(L)Cl_2](Et_4N)$, that is a 4d counterpart of the 3d complex **1** [39].

Preferable type of the JT-active distortion corresponds to one long and four short Cr-N(O) bonds in the CrN_3O_2 pentagon; comparative ligand-field calculations (see Supplementary data for detail) indicate that these distortions produce the largest energy splitting of the *xy* and x^2-y^2 orbitals and JT energy gain ΔE_{JT}. There are three types of distortions featuring different long atomic distances; Cr–N1, Cr–N2 and Cr–O1, respectively (Fig. 9b); two of them (Cr–N1 and Cr–N2) are actually observed in **1**–**11** and in other related complexes [25]. The case of the long Cr–N2 distance occurs in complexes with mono-deprotonated ligand HL^{OCH3}, where N2 is the side chelating N atom of the protonated hydrazide moiety (Fig. 3a), compounds **1**–**4** and **6**–**9** (Table 3; see also Tables S1, S3, S5, S7, S11, S12, S14 and S16). The case of the elongated

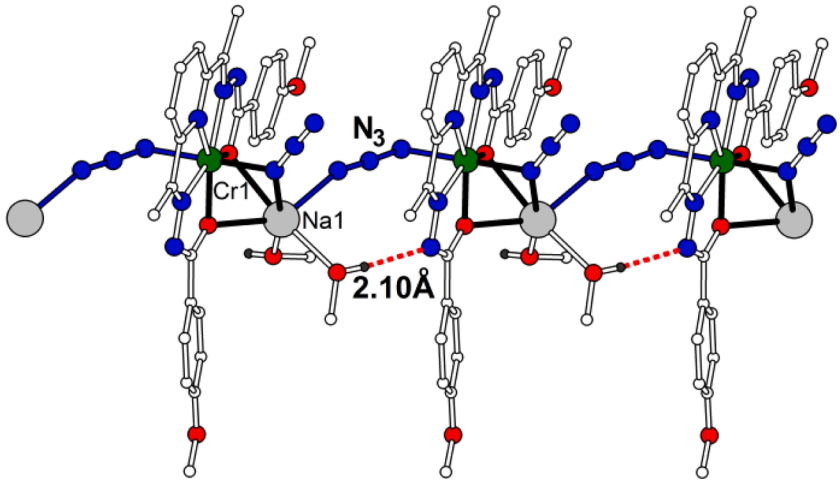

Fig. 7. Structure of the chain in **10**.

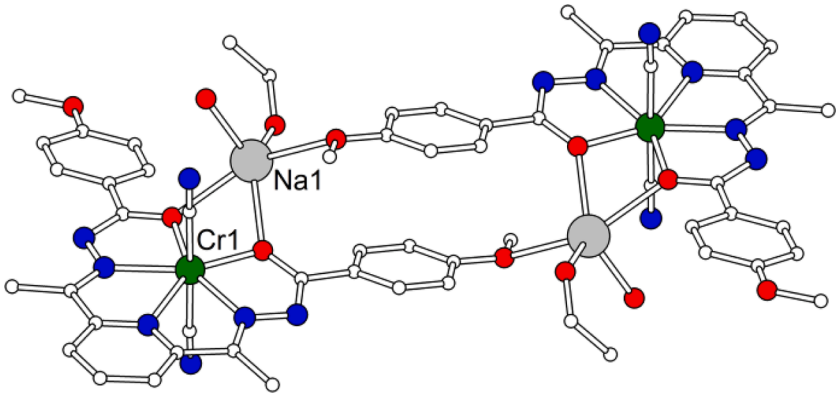

Fig. 8. Dimeric unit in **11**.

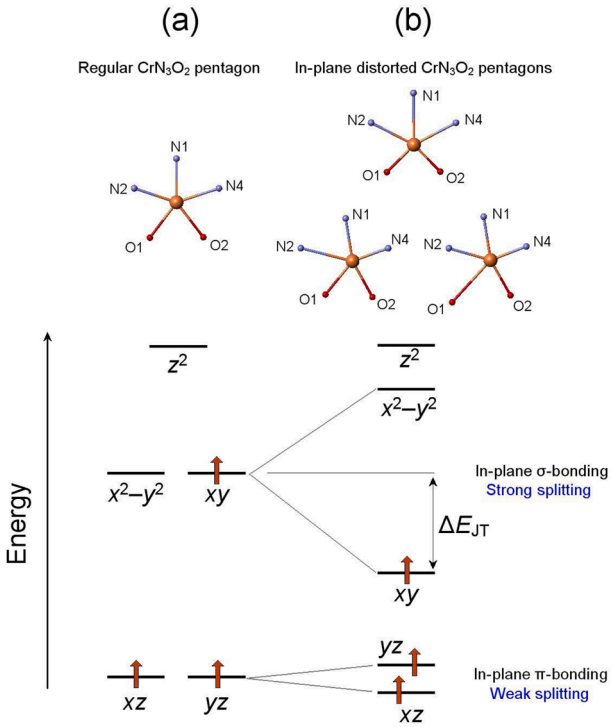

Fig. 9. On the origin of the Jahn-Teller effect in high-spin (S = 3/2) pentagonal-bipyramidal Cr(III) complexes with the central planar $Cr^{III}N_3O_2$ pentagon. The energy diagrams of 3d orbitals of Cr^{III} in (a) regular $Cr^{III}N_3O_2$ pentagon and (b) distorted $Cr^{III}N_3O_2$ pentagon are shown. In-plane shift of the central Cr atom leads to the strong energy splitting of the σ-bonding *xy* and x^2–y^2 orbitals resulting in the total energy gain of ΔE_{JT}. The JT-active types of the in-plane distortions in the $Cr^{III}N_3O_2$ pentagon are shown. They correspond to the distorted structures with long Cr-N1, Cr-N2 and Cr-O1 bonds, respectively.

Cr–N1 bond (to the coordinating N atom of pyridine ring, Fig. 3b) is found in compounds **5**, **10**, **11** with doubly-deprotonated ligand $(L^{OCH3})^{2-}$ (Tables S9, S18, S20). However, none of these compounds reveal elongated Cr-O bonds.

In order to rationalize the molecular structure of chromium PBP complexes **1**–**11**, we performed density functional theory (DFT) calculations for selected isolated $[Cr^{III}(HL^{OCH3})X_2]$ and $[Cr^{III}(L^{OCH3})X_2]$ molecules using the ORCA 3.0.3 suite of programs and employing the spin-unrestricted method at the B3LYP(BP86)/SVP(TzVPP) level of theory [52]. The DFT-optimized geometries are well consistent with the main structural features of complexes **1**–**11** with mono- and doubly deprotonated ligand H_2L^{OCH3}; the results of calculations are exemplified in Fig. 10 for isolated complexes $[Cr^{III}(HL)(H_2O)_2]^{2+}$ and $[Cr^{III}(L)(CN)_2]^-$ representing compounds **4** and **11**, respectively. In particular, for complexes with mono-deprotonated ligand DFT calculations correctly predict the elongated Cr-N2 bond at the protonated hydrazide fragment N2-N3H (Fig. 10a); for doubly deprotonated complexes they result in elongated Cr-N1 bond involving the N atom of pyridine ring (Fig. 10b). In both cases, DFT-optimized structures well describe the in-plane character of the JT distortions and reproduce their amplitude. Note that protonation of a single hydrazide group of $[HL^{OCH3}]$ may enhance distortions, albeit it is seemingly less important than the JT effect, as evidenced by DFT calculations, which indicate strong distortions in the plane in both doubly deprotonated and mono deprotonated PBP Cr(III) complexes.

Apart from these two types of distortion, DFT calculations also predict the Cr-O1 type of distortion that is not observed experimentally in **1**–**11**. Namely, geometry optimization calculations for the free high-spin (S = 3/2) molecule $[Cr^{III}(HL^{OCH3})Cl_2]$ resulted in a planar structure of the $Cr^{III}N_3O_2$ pentagon, which is strongly distorted (Fig. S19). In fact, the Cr^{III} ion is four-coordinated in the equatorial plane due to the very long Cr-O1 distance of 2.745 Å arising from the in-plane shift and rotation of the 4-methoxyphenyl group (Fig. S19). This structure differs considerably from the experimental crystal structure of **1**, which reveals the long Cr-N2 distance instead of Cr-O1 (Figs. 1 and 3a). The difference is likely due to the crystal packing effect that fixes the side phenyl groups of the HL^{OCH3} ligand and prevents them from rotations and displacements thereby blocking formation of the Cr-O1 type of distortion.

4.1. Magnetic properties

Magnetic properties were explored for compound **1** as a representative of the family of Cr(III) complexes **1**–**11**. Static magnetic susceptibility (χ) data were collected for compound **1** using a direct current (dc) field of 0.1 T over the temperature range of 2–300 K. Above 15 K, the χT product reaches a nearly constant value around 1.9 $cm^3mol^{-1}K$, which is close to the 1.875 $cm^3mol^{-1}K$ value expected for free or weakly coupled $S = 3/2$ spin system with $g = 2.0$ (Fig. 11). The high-spin nature of the ground state of chromium complex **1** is also evidenced by measurements of the magnetization at 2, 3 and 5 K, which is 2.87, 2.82 and 2.65 μ_B, respectively (under a field of 9 T, see inset in Fig. 11), being close to the saturation value of 3 μ_B for uncoupled spin $S = 3/2$. Below 6 K, χT drops to ~ 1.1 $cm^3mol^{-1}K$, presumably due to zero-field splitting (ZFS) and/or antiferromagnetic (AF) intermolecular interactions.

To get more insight into magnetic interactions underlying magnetic behavior of **1**, we simulated magnetic susceptibility, performed ligand-field (LF) calculations and explored the mechanism of the intermolecular spin coupling between the $[Cr^{III}(HL^{OCH3})Cl_2]$ units using super-exchange calculations. Primary analysis of the magnetic susceptibility shows that at low temperature the χT vs. T curve is not reproduced in terms of the single-ion ZFS model. This is also consistent with the fact

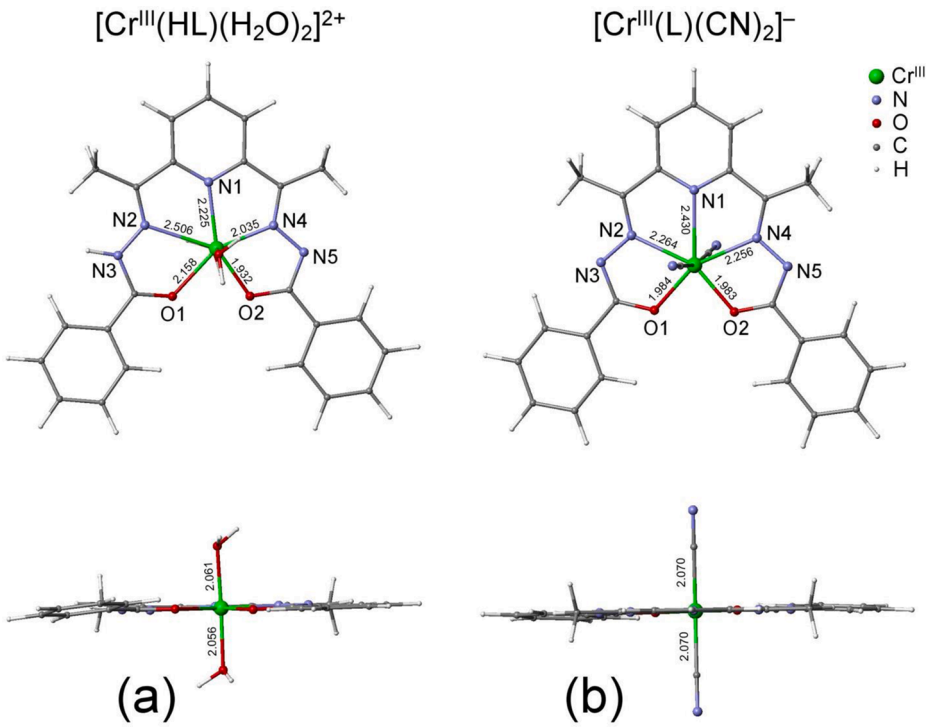

Fig. 10. Molecular structure of isolated complexes (a) $[Cr^{III}(HL)(H_2O)_2]^{2+}$ and (b) $[Cr^{III}(L)(CN)_2]^{-}$ obtained from DFT geometry optimization calculations (at the BP86/SVP(TzVPP) level). Atomic distances are indicated in Å. The calculated structure of the $Cr^{III}N_3O_2$ pentagon is well consistent with those in compounds **4** and **11** (Figs. S6, S17 and Tables S7, S20).

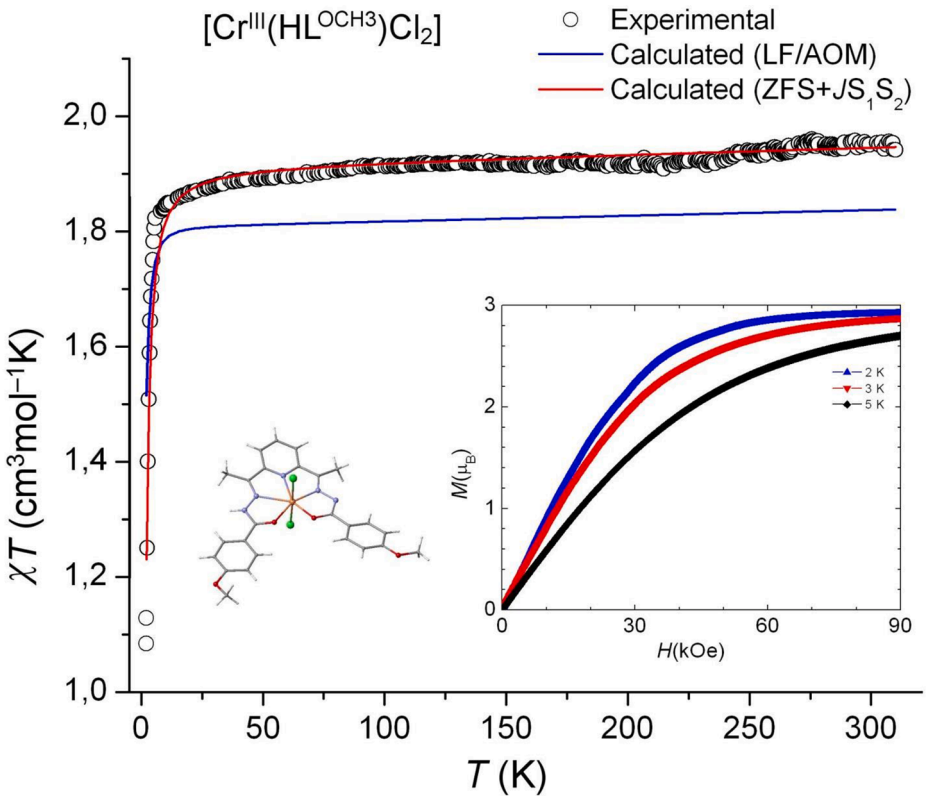

Fig. 11. Experimental (open circles) and calculated (solid lines) temperature dependence of the χT product of **1**. The solid blue line is the χT vs. T plot obtained from LF/AOM calculations (see Supplementary data for detail), the solid red line represents the χT product calculated with the ZFS + JS_1S_2 model at $D = -1.8$ cm^{-1}, $J = -0.23$ cm^{-1}, $g = 2.02$ and $\chi_{TIP} = 1.12 \cdot 10^{-4}$ cm^{3}mol^{-1}. In the inset: field dependence of magnetization at 2, 3, and 5 K.

that the χT product derived from LF calculations (combined with the angular-overlap model (AOM) [53,54], see Supplementary data for detail) differs considerably from the experimental data (blue line in Fig. 11). The LF/AOM calculations result in the ZFS parameter of $|D|$ =1.06 cm^{-1} (see Supplementary data), g = 1.963 and temperature-independent paramagnetism (TIP) of χ_{TIP} = 0.98·10^{-4} cm^3mol^{-1}. These results indicate that deep fall of χT below 6 K is likely caused by some AF spin coupling between distant Cr^{III} ions in compound **1**, which acts in concert with the single-ion ZFS mechanism. To obtain more in-depth information, we explored the mechanism of spin coupling between the $[Cr^{III}(HL^{OCH3})Cl_2]$ units in **1** in terms of a microscopic model based on the many-electron superexchange theory [36,41,55,56] (see Supplementary data for the theoretical approach and computational detail).

The structure of compound **1** is built of zig-zag chains involving two chromium pairs with short (7.43 Å) and long (8.21 Å) Cr…Cr distances (Fig. S20). In these pairs, the $[Cr^{III}(HL^{OCH3})Cl_2]$ complexes have coplanar equatorial planes CrN_3O_2 which contact via the π-stacking of the macrocyclic rings of planar HL^{OCH3} ligands (Fig. S21b,c). Our superexchange calculations show that these contacts provide efficient exchange pathway between S = 3/2 spins of Cr(III) ions in the chains (Fig. S21), which result in AF spin coupling of J = –0.09 cm^{-1} for the short pair (Cr…Cr = 7.43 Å, pair 1 shown in Fig. S21b) and J = –0.28 cm^{-1} for the long pair (Cr…Cr = 8.21 Å, Fig. S21c). These results suggest that the dimer-like spin coupling model (involving only the dominant AF spin coupling J = –0.28 cm^{-1} in the long pairs with Cr…Cr = 8.21 Å, Fig. S21c) is a good approach to describe magnetic properties of **1**. However, calculations in the frame of this model reveal an interesting feature that the outcome depends on the sign of the ZFS parameter D, while in the ZFS-only model χT is independent on the sign of D. In order to specify the sign of D, we performed LF/AOM calculations of the angular dependence of magnetization for isolated $[Cr^{III}(HL^{OCH3})Cl_2]$ molecule, which indicate the negative sign, D = –1.06 cm^{-1} (Fig. S20a). Interestingly, despite significant in-plane distortions in **1**, the calculated azimuthal anisotropy of the magnetization $M(\varphi)$ in the equatorial plane CrN_3O_2 is rather weak (Fig. S20b), which indicates axial symmetry of the ZFS tensor ($E \ll D$). Then, starting from the calculated parameters (D = –1.06 cm^{-1}, J = –0.28 cm^{-1}, g = 1.963 and χ_{TIP} = 0.98·10^{-4} cm^3mol^{-1}), the best fit for the χT vs. T data is obtained at D = –1.8 cm^{-1}, J = –0.23 cm^{-1}, g = 2.020 and χ_{TIP} = 1.12·10^{-4} cm^3mol^{-1} (Fig. 11, the solid red line); the enhanced g-factor (2.02, as opposite to $g < 2$ expected for Cr^{III}) is applied in order to absorb some uncertainty in the concentration of spin carriers in powder samples of **1** used in dc magnetic measurements. The magnitude of the calculated axial ZFS parameter in **1** is consistent with the D values in the order of |1–2| cm^{-1} for the related five complexes $[Cr^{III}(L^{N3O2R})X_2]$ previously reported in [25]. In this respect, it is relevant to note that $[Cr^{III}(HL^{N3O2Ph2})(NCS)_2]$·MeCN (compound 5 in ref. [25]) reveals a magnetic behavior similar to that of **1**, namely, its χT products sharply decreases to ca. 1.1 $cm^3mol^{-1}K$ at low temperature (Fig. S11 in [25]). As in the case of our complex **1**, such decrease cannot be attributed solely to the ZFS, especially considering that other mononuclear complexes $[Cr^{III}(L^{N3O2R})X_2]$ (indexed under 1–4 in [25]) show weak decrease in χT at low temperature (Fig. S11 in [25]). Therefore, similarly to **1**, magnetic behavior of 5 in ref. [25] may be due to AF spin coupling mediated by π-stacking of planar $HL^{N3O2Ph2}$ ligands of the neighboring $[Cr^{III}(HL^{N3O2Ph2})(NCS)_2]$ units (Fig. SI5 in [25], crystal structure CCDC 1561582); different magnetic behavior of 1–4 [25] correlates with the absence of π-stacking in their molecular structures (CCDC 1561578–1561581).

This analysis reveals complicated nature of magnetic behavior of $[Cr^{III}(HL^{OCH3})X_2]$ complexes resulting from the interplay of ZFS on chromium(III) centers and AF spin coupling between distant Cr^{III} ions mediated through the π-stacking of HL^{OCH3} ligands. A similar scheme of magnetic interactions has recently been found for related vanadium(III) PBP complexes $[V^{III}(HL)X_2]$ [57]. There were also other reports in the literature on coordination compounds composed of isolated 3d metal complexes, in which pronounced long-range spin coupling is conducted by π-stacking contacts of planar equatorial ligands [58].

5. Conclusion

We found that the reaction of the H_2DAPMBH (H_2L^{OCH3}), 2,6-diacetylpyridine bis(4-methoxybenzoylhydrazone) - a new pentadentate pyridine-base $[N_3O_2]$ ligand with $CrCl_2·4H_2O$ in methanol or $CrCl_3·6H_2O$ in CH_3CN led to a novel seven-coordinate complex $[Cr^{III}(HL^{OCH3})Cl_2]$·solv, with the mono deprotonated form of the H_2L^{OCH3} ligand. In this compound, the equatorial pentadentate ligand is very strongly bound to the metal, while axial Cl ligands easily enter into substitution reactions. Taking advantage of lability of the axial coordination positions, we obtained and characterized a number of new PBP Cr (III) complexes with different axial ligands (viz. Cl^-, CH_3O^-, N_3^-, CN^-, NCS^-). In the case of an azide axial ligand, three phases of the complex $[Cr^{III}(HL^{OCH3})(N_3)_2]·xH_2O$ composition (x = 0 or 0.2) were identified in the same batch. Analysis of the crystal structures of these compounds showed that the PBP blocks are prone to combine into dimers or polymers, either due to strong hydrogen bonds or due to the conversion of terminal ligands to bridging between various metal centers. The possibility to change the axial ligands without changing the crystal field symmetry around the Cr(III) ions provides an opportunity to use these complexes as robust magnetic building blocks for the construction of multimetallic SMMs. The key reason of strong in-plane distortions around Cr(III) ions in the PBP $Cr^{III}(3d^3)$ complexes **1**–**11** is the strong first-order Jahn-Teller effect resulting from the in-plane σ–bonding interactions for singly occupied degenerate xy, x^2-y^2 orbitals. DC magnetic measurements for complex $[Cr(HL^{OCH3})Cl_2]·4CHCl_3$ (**1**) indicate a high-spin (S = 3/2) ground state of Cr^{III}. Theoretical analysis of its magnetic properties reveals negative ZFS energy with the anisotropy parameter D = –1.8 cm^{-1} and weak dimer-like antiferromagnetic spin coupling J = –0.23 cm^{-1} between neighboring PBP units $[Cr^{III}(HL^{OCH3})Cl_2]$ mediated by π-stacking of planar HL^{OCH3} ligands.

Declaration of Competing Interest

The authors declare that they have no known competing financial interests or personal relationships that could have appeared to influence the work reported in this paper.

Acknowledgements

This work was supported by the Russian Science Foundation (project no. 18-13-00264). Yu. V. M. and A. B. K. acknowledge support by the Ministry of Education and Science of the Russian Federation, State task AAAA-A19-119071190045-0 (synthesis of the ligands, the Section "Synthesis and characterization"). V. S. M. acknowledges support by the Ministry of Science and Higher Education within the State assignment FSRC 'Crystallography and Photonics' RAS in part of the Jahn-Teller effect. Structural research was partially performed within the state assignment for ISSP RAS.

Appendix A. Supplementary data

Supplementary data to this article can be found online at https://doi.org/10.1016/j.ica.2021.120358.

References

[1] P. A. Lay and A. Levina "Chromium" in COMPREHENSIVE COORDINATION CHEMISTRY II, From Biology to Nanotechnology, Second Edition; Edited by J.A. McCleverty, University of Bristol, UK T.J. Meyer, Los Alamos National Laboratory, Los Alamos, USA, 331-383 and references therein.
[2] N.A.P. Kane-Maguire, Top. Curr. Chem. 280 (2007) 37–67, https://doi.org/10.1007/128_2007_141.

[3] B. Doistau, G. Collet, E.A. Bolomey, V. Sadat-Noorbakhsh, C. Besnard, C. Piguet, Inorg. Chem. 57 (2018) 14362–14373, https://doi.org/10.1021/acs.inorgchem.8b02530.
[4] G.A. Craig, M. Murrie, Chem. Soc. Rev. 44 (2015) 2135–2147, https://doi.org/10.1039/C4CS00439F.
[5] C.C. Cummins, R.R. Schrock, W.M. Davis, Organometallics 11 (1992) 1452–1454, https://doi.org/10.1021/om00040a011.
[6] S. Gómez-Coca, E. Cremades, N. Aliaga-Alcalde, E. Ruiz, Inorg. Chem. 53 (2014) 676–678, https://doi.org/10.1021/ic402256v.
[7] D. Pinkowicz, F.J. Birk, M. Magott, K. Schulte, K.R. Dunbar, Chem. Eur. J. 23 (2017) 3548–3552, https://doi.org/10.1002/chem.201605528.
[8] V.V. Novikov, A.A. Pavlov, Y.V. Nelyubina, M.-E. Boulon, O.A. Varzatskii, Y. Z. Voloshin, R.E.P. Winpenny, J. Am. Chem. Soc. 137 (2015) 9792–9795, https://doi.org/10.1021/jacs.5b05739.
[9] Y. Peng, T. Bodenstein, K. Fink, V. Mereacre, C.E. Anson, A.K. Powell, Phys. Chem. Chem. Phys. 18 (2016) 30135–30143, https://doi.org/10.1039/C6CP03157A.
[10] B. Yao, Y.-F. Deng, T. Li, J. Xiong, B.-W. Wang, Z. Zheng, Y.-Z. Zhang, Inorg. Chem. 57 (2018) 14047–14051, https://doi.org/10.1021/acs.inorgchem.8b02692.
[11] B. Yao, M.K. Singh, Y.-F. Deng, Y.-N. Wang, K.R. Dunbar, Y.-Z. Zhang, Inorg. Chem. 59 (2020) 8505–8513, https://doi.org/10.1021/acs.inorgchem.0c00950.
[12] I. Ivanović-Burmazović, K. Andjelković, Adv. Inorg. Chem. 55 (2004) 315–360, https://doi.org/10.1016/S0898-8838(03)55006-1.
[13] L.J. Batchelor, M. Sangalli, R. Guillot, N. Guihéry, R. Maurice, F. Tuna, T. Mallah, Inorg. Chem. 50 (2011) 12045–12052, https://doi.org/10.1021/ic201534e.
[14] E.L. Gavey, M. Pilkington, Chem. Rev. 296 (2015) 125–152, https://doi.org/10.1016/j.ccr.2015.03.017.
[15] A.K. Mondal, A. Mondal, B. Dey, S. Konar, Inorg. Chem. 57 (2018) 9999–10008, https://doi.org/10.1021/acs.inorgchem.8b01162.
[16] Y.-F. Deng, B. Yao, P.-Z. Zhan, D. Gan, Y.-Z. Zhang, K.R. Dunbar, Dalton Trans. 48 (2019) 3243–3248, https://doi.org/10.1039/C8DT05074K.
[17] A.K. Bar, N. Gogoi, C. Pichon, D.P. Goli, M. Thlijeni, C. Duhayon, N. Suaud, N. Guihéry, A.-L. Barra, S. Ramasesha, J.-P. Sutter, Eur. Chem. J. 23 (2017) 4380–4396.
[18] A.K. Bar, C. Pichon, J.-P. Sutter, Coord. Chem. Rev. 308 (2016) 346–380, https://doi.org/10.1016/j.ccr.2015.06.013.
[19] D. Darmanović, I. N. Shcherbakov, C. Duboc, V. Spasojević, D. Hanzel, K. Anđelković, D. Radanović, I. Turel, M. Milenković, M. Gruden, B. Cobeljić, M. Zlatar, J. Phys. Chem. C 123 (2019) 31142-31155. https://doi.org/10.1021/acs.jpcc.9b08066.
[20] A.K. Bar, C. Pichon, N. Gogoi, C. Duhayon, S. Ramasesha, J.-P. Sutter, Chem. Commun. 51 (2015) 3616–3619, https://doi.org/10.1039/C4CC10182K.
[21] N. Gogoi, M. Thlijeni, C. Duhayon, J.-P. Sutter, Inorg. Chem. 52 (2013) 2283–2285, https://doi.org/10.1021/ic3027368.
[22] B. Drahoš, R. Herchel, Z. Trávníček, Inorg. Chem. 54 (2015) 3352–3369, https://doi.org/10.1021/ic503054m.
[23] U. Rychlewska, R.C. Palenik, R.W. King, G.J. Palenik, J. Chem. Soc., Chem. Commun. (1975) 799–800, https://doi.org/10.1039/C39750000799.
[24] A. Bino, R. Frim, M. van Genderen, Inorg. Chim. Acta 127 (1987) 95–101, https://doi.org/10.1016/S0020-1693(00)88368-1.
[25] C. Pichon, B. Elrez, V. Béreau, C. Duhayon, J.-P. Sutter, Eur. J. Inorg. Chem. (2018) 340–348, https://doi.org/10.1002/ejic.201700845.
[26] C. Pichon, N. Suaud, C. Duhayon, N. Guihéry, J.-P. Sutter, J. Am. Chem. Soc. 140 (2018) 7698–7704, https://doi.org/10.1021/jacs.8b03891.
[27] K. Bretosh, V. Béreau, C. Duhayon, C. Pichon, J.-P. Sutter, Inorg. Chem. Front. 7 (2020) 1503–1511, https://doi.org/10.1039/C9QI01489F.
[28] S. Inoue, H. Koinuma, T. Tsuruta, J. Polym. Sci. Part B Polym. Lett. 7 (1969) 287–292, https://doi.org/10.1002/pol.1969.110070408.
[29] M.I. Childers, J.M. Longo, N.J. van Zee, A.M. LaPointe, G.W. Coates, Chem. Rev. 114 (2014) 8129–8152, https://doi.org/10.1021/cr400725x.
[30] S. Paul, Y.Q. Zhu, C. Romain, R. Brooks, P.K. Saini, C.K. Williams, Chem. Commun. 51 (2015) 6459–6479, https://doi.org/10.1039/C4CC10113H.
[31] G.A. Luinstra, Polym. Rev. 48 (2008) 192–219, https://doi.org/10.1080/15583720701834240.
[32] D.J. Darensbourg, Chem. Rev. 107 (2007) 2388–2410, https://doi.org/10.1021/cr068363q.
[33] O.M. Chukanova, T.A. Bazhenova, Y.V. Manakin, A.B. Kornev, I.V. Sedov, Complexes of metals with pentadentant (N3O2) ligands, a method for their preparation, catalytic systems for carrying out reactions of carbon dioxide with epoxides, a method for producing cyclic carbonates or aliphatic polycarbonates, Patent of Russian Federation no. 2740944/03 (2021).
[34] V.S. Mironov, L.F. Chibotaru, A. Ceulemans, J. Amer. Chem. Soc. 125 (2003) 9750–9760, https://doi.org/10.1021/ja029518o.
[35] V. S. Mironov, Dokl. Phys. Chem. 408 (2006) 130-136. https://doi.org/10.1134%2FS001250160605006X.
[36] V.S. Mironov, Inorg. Chem. 54 (2015) 11339–11355, https://doi.org/10.1021/acs.inorgchem.5b01975.
[37] V.S. Mironov, Inorganics 6 (2018) 58, https://doi.org/10.3390/inorganics6020058.
[38] V.S. Mironov, T.A. Bazhenova, Y.V. Manakin, K.A. Lyssenko, A.D. Talantsev, E. B. Yagubskii, Dalton Trans. 46 (2017) 14083–14087, https://doi.org/10.1039/C7DT02912H.
[39] Y.V. Manakin, V.S. Mironov, T.A. Bazhenova, K.A. Lyssenko, I.F. Gilmutdinov, K. S. Bikbaev, A.A. Masitov, E.B. Yagubskii, Chem. Commun. 54 (2018) 10084–10087, https://doi.org/10.1039/C8CC06038J.
[40] T.A. Bazhenova, V.S. Mironov, I.A. Yakushev, R.D. Svetogorov, O.V. Maximova, Y. V. Manakin, A.B. Kornev, A.N. Vasiliev, E.B. Yagubskii, Inorg. Chem. 59 (2020) 563–578, https://doi.org/10.1021/acs.inorgchem.9b02825.
[41] V.D. Sasnovskaya, V.A. Kopotkov, A.D. Talantsev, R.B. Morgunov, E.B. Yagubskii, S.V. Simonov, L.V. Zorina, V.S. Mironov, Inorg. Chem. 56 (2017) 8926–8943, https://doi.org/10.1021/acs.inorgchem.7b00676.
[42] V.D. Sasnovskaya, V.A. Kopotkov, A.V. Kazakova, A.D. Talantsev, R.B. Morgunov, S.V. Simonov, L.V. Zorina, V.S. Mironov, E.B. Yagubskii, New J. Chem. 42 (2018) 14883–14893, https://doi.org/10.1039/C8NJ01928B.
[43] L.V. Zorina, S.V. Simonov, V.D. Sasnovskaya, A.D. Talantsev, R.B. Morgunov, V. S. Mironov, E.B. Yagubskii, Chem. Eur. J. 25 (2019) 14583–14597, https://doi.org/10.1002/chem.201902551.
[44] T.J. Giordano, G.J. Palenik, R.C. Palenik, D.A. Sullivan, Inorg. Chem. 18 (1979) 2445–2450, https://doi.org/10.1021/ic50199a023.
[45] Rigaku: Tokyo, Japan (2015).
[46] G.M. Sheldrick, Acta Crystallogr, Sect. A: Found. Crystallogr. 64 (2008) 112–122, https://doi.org/10.1107/S0108767307043930.
[47] L. Palatinus, G. Chapuis, J. Appl. Crystallogr. 40 (2007) 786–790, https://doi.org/10.1107/S0021889807029238.
[48] Larkworthy, O. F.; Nolan, K. B.; O'Brien, P. In Comprehensive Coordination Chemistry; Wilkinson, G., Gillard, R. D. and McCleverty, J. A., Eds.; Pergamon Press: Oxford, 1987; Vol. 3, 699-969 and references therein.
[49] H. Hosseini-Monfared, R. Bikas, M. Siczek, T. Lis, R. Szymczak, P. Aleshkevych, Inorg. Chem. Commun. 35 (2013) 172–175, https://doi.org/10.1016/j.inoche.2013.06.009.
[50] H. Hosseini-Monfared, R. Bikas, R. Szymczak, P. Aleshkevych, A.M. Owczarzak, M. Kubicki, Polyhedron 63 (2013) 74–82, https://doi.org/10.1016/j.poly.2013.06.055.
[51] F.A. Mautner, C. Berger, R.C. Fischer, S.S. Massoud, R. Vicente, Polyhedron 134 (2017) 126–134, https://doi.org/10.1016/j.poly.2017.06.025.
[52] F. Neese, Wiley Interdiscip. Rev.: Comput. Mol. Sci. 2 (2012) 73–78, https://doi.org/10.1002/wcms.81.
[53] C.E. Schaeffer, C.K. Jorgensen, Mol. Phys. 9 (1965) 401–412, https://doi.org/10.1080/00268976500100551.
[54] C.E. Schaffer, Struct. Bonding 5 (1968) 68–95, https://doi.org/10.1007/BFb0118847.
[55] V.S. Mironov, L.F. Chibotaru, A. Ceulemans, Phys. Rev B. 67 (2003), 014424, https://doi.org/10.1103/PhysRevB.67.014424.
[56] E.N. Zorina, N.V. Zauzolkova, A.A. Sidorov, G.G. Aleksandrov, A.S. Lermontov, M. A. Kiskin, A.S. Bogomyakov, V.S. Mironov, V.M. Novotortsev, I.L. Eremenko, Inorg. Chim. Acta. 396 (2013) 108–118, https://doi.org/10.1016/j.ica.2012.10.016.
[57] T.A. Bazhenova, L. Zorina, S. Simonov, V.S. Mironov, O. Maximova, L. Spillecke, C. Koo, R. Klingeler, Y. Manakin, A.N. Vasiliev, E.B. Yagubskii, Dalton Trans. 49 (2020) 15287–15298, https://doi.org/10.1039/D0DT03092A.
[58] V. Tangoulis, M. Lalia-Kantouri, M. Gdaniec, C.h. Papadopoulos, V. Miletic, A. Czapik, Inorg. Chem. 52 (2013) 6559–6569, https://doi.org/10.1021/ic400557f.